Clim. Past Discuss., 9, 3321–3370, 2013
www.clim-past-discuss.net/9/3321/2013/
doi:10.5194/cpd-9-3321-2013


Climate of the Past Discussions



# Sources and transport of dust to East Antarctica: new insights from high-resolution terrestrial and marine aerosol records from the Talos Dome ice core

**S. Schüpbach**[1,2,3], **U. Federer**[1,2], **S. Albani**[4], **C. Barbante**[3,5], **T. F. Stocker**[1,2], **and H. Fischer**[1,2]

[1]Climate and Environmental Physics, Physics Institute, University of Bern, Bern, Switzerland
[2]Oeschger Centre for Climate Change Research, University of Bern, Bern, Switzerland
[3]Environmental Sciences, Informatics and Statistics Department, University of Venice, Venice, Italy
[4]Department of Earth and Atmospheric Sciences, Cornell University, Ithaca, NY, USA
[5]Institute for the Dynamics of Environmental Processes - National Research Council, Venice, Italy



Received: 31 May 2013 – Accepted: 16 June 2013 – Published: 21 June 2013

Correspondence to: S. Schüpbach (schuepbach@climate.unibe.ch)

Published by Copernicus Publications on behalf of the European Geosciences Union.

**Abstract**

In this study we report on new non-sea salt calcium ($nssCa^{2+}$, mineral dust proxy) and sea salt sodium ($ssNa^{+}$, sea ice proxy) records along the East Antarctic Talos Dome deep ice core in centennial resolution reaching back 150 thousand years before present. During glacial conditions $nssCa^{2+}$ fluxes in Talos Dome are strongly related to temperature as has been observed before in other deep Antarctic ice core records, and has been associated with synchronous changes in the main source region (southern South America) during climate variations in the last glacial. However, during warmer climate conditions Talos Dome mineral dust input is clearly elevated compared to other records mainly due to the contribution of additional local dust sources in the Ross Sea area. Based on a simple transport model we compare $nssCa^{2+}$ fluxes of different East Antarctic ice cores. From this multi-site comparison we conclude that changes in transport efficiency or atmospheric lifetime of dust particles do have a minor effect compared to source strength changes on the large scale concentration changes observed in Antarctic ice cores during climate variations of the past 150 thousand years. Our transport model applied on ice core data only so far is further validated by climate model data. The availability of multiple East Antarctic $nssCa^{2+}$ records allows for a revision of a former estimate on the atmospheric $CO_2$ sensitivity to reduced dust induced iron fertilisation in the Southern Ocean (SO) during the transition from the Last Glacial Maximum to the Holocene (T1). While the former estimate based on the EDC record only suggested 20 ppm, we find reduced dust induced iron fertilisation in the SO to be responsible for up to 40 ppm of the total atmospheric $CO_2$ increase during T1. During the last interglacial, $ssNa^{+}$ levels of EDC and EDML are only half of the Holocene levels, in line with higher temperatures during that period, indicating much reduced sea ice extent in the Atlantic as well as the Indian Ocean sector of the SO. In contrast, Holocene $ssNa^{+}$ flux in Talos Dome is about the same as during the last interglacial, indicating that there was similar ice cover present in the Ross Sea area during MIS 5.5 as during the Holocene.



## 1 Introduction

Long and detailed climate records obtained from deep ice cores drilled on the East Antarctic ice sheet allow to assess the past climate variability on a variety of parameters and timescales at high southern latitudes (e.g. Petit et al., 1999; EPICA, 2004; Brook et al., 2005; EPICA, 2006; Jouzel et al., 2007). Such climate reconstructions are considered representative for the entire southern high latitude region including Antarctica and the Southern Ocean (SO), which plays a crucial role in glacial/interglacial changes and in fast climate changes during the last glacial period (Blunier et al., 1997; Knorr and Lohmann, 2003; Stocker and Johnsen, 2003; EPICA, 2006), as well as in the global carbon cycle (Archer et al., 2000; Toggweiler et al., 2006; Fischer et al., 2010; Bereiter et al., 2012). Despite the variety of such climate records from Antarctic ice cores, information on accompanying regional environmental changes is still limited. Thus, detailed information on e.g. enhanced phytoplankton productivity through atmospheric dust deposition in the SO (iron fertilisation) (Martin, 1990) could contribute to a better understanding of the impact of regional climate changes on the global carbon cycle. Also sea ice in the SO is a key component of the southern high latitude climate system, because an increase in its extent increases the albedo of the ocean, reduces gas exchange, and decreases ocean mixing. It plays a major role in the formation of deep waters in the ocean, and therefore in global ocean circulation and the carbon cycle (Toggweiler, 1999; Bouttes et al., 2010; Dieckmann and Hellmer, 2010). One possibility to assess past changes in these two parameters are aerosol records in deep Antarctic ice cores, which provide detailed information on mineral dust deposition and sea ice coverage in different regions of Antarctica (Petit et al., 1990; Röthlisberger et al., 2002; Wolff et al., 2003, 2006; Fischer et al., 2007b; Bigler et al., 2010; Abram et al., 2013).

During glacial/interglacial cycles, most of the variability in atmospheric dust concentration in central East Antarctica was related to the strength of remote continental mineral dust sources and to the atmospheric transport efficiency (Fischer et al., 2007b;

Petit and Delmonte, 2009). Southern South America (SSA) (i.e. southern Patagonia) is believed to be the most important source region for glacial terrestrial aerosols to East Antarctica (Basile et al., 1997; Gaiero, 2007; Delmonte et al., 2008; Gabrielli et al., 2010), whereas during the Holocene other remote sources become relatively more important for the dust input to East Antarctica due to the strong decline in dust mobilization in Patagonia (Revel-Rolland et al., 2006; Li et al., 2008; Marino et al., 2009; Gabrielli et al., 2010; Wegner et al., 2012). In addition, dust sources from ice-free areas in the periphery of Antarctica may also contribute. While for high-altitude drill sites on the interior of the East Antarctic plateau (e.g. Vostok, EDC) such local sources may be insignificant, their contribution becomes more important for peripheral areas (Bory et al., 2010; Delmonte et al., 2010b; Albani et al., 2012a), in particular those close to the Transantarctic Mountains. Thus, the TALDICE (TALos Dome Ice CorE) project located at Talos Dome in the Ross Sea sector of East Antarctica in Northern Victoria land (72°70′ S, 159°11′ E) (Frezzotti et al., 2007; Stenni et al., 2011) provides a well-suited deep ice core to investigate in detail the regional atmospheric circulation changes and their relationship with the glaciation history and environmental changes in the Ross Sea area for the past two glacial/interglacial cycles based on climate as well as terrestrial and sea salt aerosol records.

Physical-chemical properties of dust analysed in Talos Dome snow and ice suggest that local contribution (unconsolidated glacial deposits e.g. in the Antarctic Dry Valleys and regolith located at high elevation in Northern Victoria Land) to Aeolian dust input was increasing during the Holocene when dust input from remote sources was low compared to the Last Glacial period (Delmonte et al., 2010b; Albani et al., 2012a; Delmonte et al., 2013). Dust deflation and transport from proximal sources to the Talos Dome site is influenced by the availability and strength of the dust sources as well as by local meteorological conditions, which in turn are related to regional climate (Albani et al., 2012a). Despite the importance of Aeolian dust transport to Antarctica, information on sources and transport of mineral dust from peripheral ice-free areas towards the Antarctic interior is still limited. One major difficulty to assess the spatial extent of local



dust sources by means of analyses of the isotopic composition of strontium ($^{87}Sr/^{86}Sr$) and neodymium ($^{143}Nd/^{144}Nd$) of the Aeolian dust is its extremely low concentration in ice cores during interglacial climate conditions (Petit and Delmonte, 2009; Delmonte et al., 2013).

Sea salt aerosol production is related to the presence of sea ice on the surface of which brine and frost flower formation (on freshly formed or submerged sea ice) and blowing snow are suggested to be the most relevant sea salt aerosol sources (Wagenbach et al., 1998; Rankin et al., 2000; Wolff et al., 2003; Yang et al., 2008; Abram et al., 2013). Thus sea salt aerosol input on the East Antarctic plateau should be linked to the sea ice extent in the SO. Sea salt aerosol source regions for the Atlantic and Indian Ocean sector of Antarctica are not the same and source strength as well as transport may have changed independently in different regions around Antarctica. Accordingly, we interpret sea salt aerosol here as a sea ice proxy restricted to the closest source area, thus the Atlantic Ocean sector of the SO for EDML, the Indian Ocean sector for EDC and Vostok, and the Ross Sea sector for TALDICE, as indicated by back trajectory calculations (Reijmer et al., 2002; Scarchilli et al., 2011) and by the limited atmospheric lifetime of the sea salt aerosol (Fischer et al., 2007b; Röthlisberger et al., 2010).

In this study we report on mineral dust represented by non-sea salt calcium ($nssCa^{2+}$) and sea salt aerosol represented by sea salt sodium ($ssNa^{+}$) records from TALDICE in centennial resolution reaching back 150 thousand years before present (ka BP). The new aerosol data from TALDICE is in the following compared with three other East Antarctic ice core records, all covering at least the past 150 ka (a map of Antarctica with all investigated ice core sites is shown in Fig. 1). These are the two deep ice cores drilled within the European Project for Ice Coring in Antarctica (EPICA) at Dome C – EDC, 75°06′ S, 123°21′ E, 3233 m a.s.l. (above sea level) – (EPICA, 2004) and at Kohnen station in Dronning Maud Land (EDML, 75°00′ S, 00°04′ E, 2882 m a.s.l.) (EPICA, 2006), as well as the Vostok ice core (78°28′ S, 106°50′ E, 3488 m a.s.l.) (Petit et al., 1999). Fischer et al. (2007a) have shown that a comparison of $nssCa^{2+}$ records

of different ice cores can reveal substantial information about the sources and transport mechanisms of dust deposited on the East Antarctic plateau. Here we aim at complementing the findings by Fischer et al. (2007a) by a multi-site comparison of nss$Ca^{2+}$ ice core records in centennial resolution, complemented with model data of dust deposition on the East Antarctic plateau available for the Last Glacial Maximum (LGM) and Holocene. The ss$Na^{+}$ records of the different drill sites give indications on the evolution of local sea ice coverage in the Atlantic Ocean, Indian Ocean, and Ross Sea sector of the SO during the past 150 ka BP.

## 2 Materials and methods

### 2.1 Data acquisition and performance

This study is based on high-resolution aerosol data from the Antarctic ice cores EDC (Röthlisberger et al., 2004; Bigler et al., 2006, 2010), EDML (Fischer et al., 2007a; Kaufmann et al., 2010), and TALDICE (new data), respectively. All analyses were performed using Continuous Flow Analysis (CFA) (Röthlisberger et al., 2000; Kaufmann et al., 2008). Besides these high-resolution data we included $Na^{+}$ and $Ca^{2+}$ records of the Vostok ice core in our multi-site comparison, which are available in coarse resolution only (De Angelis et al., 1997) and are based on discrete ion chromatographic (IC) analysis of samples after manual decontamination.

CFA analyses of Calcium ($Ca^{2+}$) and Sodium ($Na^{+}$) of TALDICE have been performed in the years 2006–2008 at the Alfred-Wegener-Institut (AWI) in Bremerhaven, Germany. The covered depth interval (305–1435 m) corresponds to an age interval of 3.8–150 ka BP. Major gaps in the new TALDICE datasets can be found in the $Ca^{2+}$ record from 490–502 m and from 535–578 m, as well as in the $Na^{+}$ record from 441–449 m, respectively. Apart from the mentioned gaps no gaps longer than 5 consecutive meters can be found in either of the new records (see Fig. 2). The before mentioned longer gaps are due to failure and maintenance of the respective detector while CFA



measurements where continued. Other smaller gaps are present mainly due to bad ice quality (mostly in the brittle ice zone) or distinct visible (ash) layers which were not processed with CFA. Apart from these gaps continuous records have been achieved with a sampling resolution of 0.5 cm or better. Due to signal dispersion in the CFA system the effective depth resolution is 1 cm ($Ca^{2+}$) and 2 cm ($Na^{+}$), respectively, at a melt speed of approx. 4 cm $min^{-1}$ as it was applied during the TALDICE analyses (Kaufmann et al., 2008). Limit of detections (LOD) are 0.1 ppbw for $Ca^{2+}$ and 0.5 ppbw for $Na^{+}$, respectively, measurement errors are estimated to be generally below 10 % (Röthlisberger et al., 2000; Kaufmann et al., 2008). Especially the very low LOD is a consequence of the continuous melt decontamination accomplished by CFA, which reduces process blanks considerably compared to manual ice sample decontamination for IC measurements.

EDML $Na^{+}$ data in the age interval 123.3–132.3 ka BP (depth: 2341–2383 m) have been analysed using IC (Fischer et al., 2007a) in 1 m resolution due to missing CFA $Na^{+}$ data in this depth interval.

On the Vostok ice core 237 discontinuous measurements have been analysed with a mean depth resolution of 10.1 m, using IC only (De Angelis et al., 1997). Each individual ice sample, once decontaminated by rinsing, was generally 10 cm long. Of these measurements, covering a depth range 100–2500 m, we show 218 data points which are within an age range of 5–150 ka BP for our multi-site comparison, resulting in a mean age resolution of 665 yr.

### 2.2 Data treatment and dating

In order to compare the different ice cores properly the different resolutions of the data sets have to be considered. Therefore equally distributed age means (100 and 500 yr, respectively, for all the high-resolution records, and 500 yr only for the Vostok records) were calculated for all four ice cores using the well-synchronised recent AICC2012 age scales (Bazin et al., 2012; Veres et al., 2012). In the following we describe how this

is achieved based on the three high-resolution records and the discrete IC records of Vostok ice core, respectively.

The age scale used for the four ice cores Vostok, EDC, EDML, and TALDICE, respectively, is the AICC2012 age scale (Bazin et al., 2012; Veres et al., 2012). The internal synchronisations of these four ice cores result in very high consistency of the age scales as far back as 150 ka BP, which allows for a direct comparison of the records. All ages are indicated in 1000 yr before present (ka BP), where present refers to 1950 AD.

The age scale (given in 1–3 m resolution, depending on the ice core and depth range, respectively) has been interpolated to assign an age to each individual data point of the high-resolution records. In the same way the accumulation rates have been interpolated in order to calculate deposition fluxes and to reconstruct the atmospheric signals (see next section). Centennial medians have then been calculated from the high-resolution data on the common age scale for each record. Medians have been calculated to prevent the hundred year mean values from being biased by single extreme events. The number of high-resolution data points per 100 yr interval ranges from 6000 (Holocene) to 77 (during the penultimate glacial, i.e. 140 ka BP) due to the increasing thinning of the ice layers towards the bottom. A threshold has been introduced when calculating the 100 yr median values: If more than one third of the high-resolution data within the interval, from which a 100 yr median has been calculated, was missing, the median has been discarded, again in order to prevent an extreme event to bias the mean value significantly. The same threshold has been applied for the calculation of the 500 yr medians.

For the Vostok records, available in coarser resolution only, we simply interpolated the age scale to assign an age to each data point at its individual depth. From these data points we then interpolated $Na^+$ and $Ca^{2+}$ concentrations to obtain a value for each 500 yr step in accordance with the 500 yr means of the three other cores. No 100 yr values have been calculated for Vostok due to the coarse resolution of the original data sets. We acknowledge that this is an inaccurate treatment from a statistical point of view; however, the records we obtain in this way are used for illustrative pur-



pose only, while the significance is in no way comparable to the records of the other three cores.

### 2.3 Reconstruction of source-separated and atmospheric signals

In addition to water-insoluble dust particles also water-soluble $Ca^{2+}$ ions can be considered as a valuable ice core proxy of continental aerosol input onto the East Antarctic ice sheet. However, not only continental sources emit $Ca^{2+}$ but also sea water can have a considerable contribution to the total $Ca^{2+}$ load in the air masses, especially during interglacial periods. Sodium on the other hand originates mainly from the marine source, but has also some continental source contribution. Thus, the sea water contribution has to be deduced from the total $Ca^{2+}$ signal in order to obtain the $nssCa^{2+}$ concentration representing continental dust input, and accordingly continental contribution is deduced from total $Na^+$ in order to obtain the $ssNa^+$ signal only. In all four ice core records the $nssCa^{2+}$ and the $ssNa^+$ fractions, respectively, are calculated from the $Ca^{2+}$ and $Na^+$ records according to Bigler et al. (2006), allowing for a direct comparison of the different ice cores.

In order to account for the dilution of the original atmospheric aerosol concentrations in the ice core samples by snow accumulation the measured concentrations have to be corrected for this effect. This is achieved by multiplying the measured concentrations by the modeled accumulation rate at the respective depth or age, respectively, resulting in the total deposition flux of the aerosol, $J(nssCa^{2+})$ and $J(ssNa^+)$, respectively (Wolff et al., 2006; Fischer et al., 2007b). For EDC, EDML, and Vostok atmospheric aerosol concentrations have been reconstructed by multiplying the $ssNa^+$ and $nssCa^{2+}$ concentration records with the accumulation rate as modeled for the AICC2012 age scale. For TALDICE we have used the accumulation rate calculated by Buiron et al. (2011) which has also been used for modeling the AICC2012 time scale of TALDICE. In low accumulation sites where the total deposition flux of an aerosol is dominated by dry deposition, the flux is essentially independent of changes in the accumulation rate and thus almost proportional to the original atmospheric aerosol concentration.

Therefore, we discuss aerosol fluxes in this study, which are more representative of the original atmospheric aerosol concentrations (Fischer et al., 2007b). It is acknowledged that in contrast to EDC (average Holocene acc. rate = 26 kg m$^{-2}$ a$^{-1}$) and Vostok (average Holocene acc. rate = 24 kg m$^{-2}$ a$^{-1}$), where dry deposition is predominant, EDML (average Holocene acc. rate = 55 kg m$^{-2}$ a$^{-1}$) and Talos Dome (average Holocene acc. rate = 73 kg m$^{-2}$ a$^{-1}$) are more intermediate accumulation sites. Thus, wet deposition can have a significant influence on the deposition fluxes, contributing to additional artificial variation in the calculated flux rates of EDML and TALDICE data used in this work. Furthermore, the uncertainties of the modeled accumulation rates are usually in the order of 20 %. Together with the estimated measurement errors of below 10 %, the uncertainties of the total flux depositions are estimated to be in the order of 30 %. Even though this estimated error is considerable, it is still small compared to glacial/interglacial nssCa$^{2+}$ flux changes in the order of one magnitude.

## 3 Results and discussion

### 3.1 The TALDICE nssCa$^{2+}$ and ssNa$^{+}$ main features

In this publication we present the first continuous high-resolution records of Ca$^{2+}$ and Na$^{+}$, respectively, of the Talos Dome ice core. Both species are conservatively deposited onto the ice sheet, thus there is no need to account for additional post-depositional effects distorting the aerosol concentrations in the ice. The concentrations of the two species are shown in Fig. 2 versus depth in 10 cm and 1 m resolution, respectively, along with the TALDICE $\delta^{18}$O profile in 1 m resolution (Stenni et al., 2011) and the modeled accumulation rate at Talos Dome. Since part of the concentration changes seen in Fig. 2 is simply due to the fact that the snow accumulation rate is changing considerably (estimated to be more than a factor of two, see 2nd panel in Fig. 2) over glacial/interglacial cycles, we will discuss the fluxes of the source separated signals in the following.



#### 3.1.1 The past 20 ka

In the middle panel of Fig. 3 J(nssCa$^{2+}$) is plotted for the past 150 ka. Distinct changes in the flux rates can be observed along with major changes in temperature (top panel in Fig. 3). However, it can be seen that these flux rate changes are much less pronounced in TALDICE than in the other cores. This is most evident for J(nssCa$^{2+}$) during glacial/interglacial transitions where flux rate changes of a factor of 4 are prevailing for TALDICE (see Table 1). As a comparison, the glacial/interglacial flux rate changes are in the order of a factor of 20 for EDC and EDML, respectively. The rather high Holocene values are in line with previous results of dust and iron flux, respectively, in TALDICE (Albani et al., 2012a; Vallelonga et al., 2013), and also show a comparable shape. After a minimum at around 12–13 ka BP during the Antarctic Cold Reversal (ARC), J(nssCa$^{2+}$) increases again during the early Holocene in the TALDICE record. The flux values show a maximum at about 8 ka BP after which they decrease continuously (see Fig. 4). The other two cores show a similar behavior during the Holocene, however at a much lower level and with much less distinct flux rate changes compared to TALDICE. This behavior might point to additional dust sources proximal to the TALDICE drill site becoming available at the beginning of the Holocene, e.g. from glacial drift left behind from retreating glaciers during the retreat of the Ross Ice Sheet between 13 and 9 ka BP. Afterwards, the efficient new sources might get more and more depleted, leading to a steady decrease of dust input from these sources during the mid-Holocene. Such a steady depletion of the local dust source would be expected to be accompanied by a coeval shift within the dust grain size distribution, i.e. an increasing contribution of smaller particles. However such a behaviour is not corroborated by dust particle size distributions as pointed out by Albani et al. (2012a), who report variable but rather constant dust grain size distribution after the deglaciation. Instead, they suggest that the retreat of the Ross Ice Shelf $\approx$ 8 ka BP and the coeval opening of the Ross Sea embayment could have caused a modification of the regional atmospheric circulation patterns. The distribution of air mass trajectories after 8 ka BP was less favourable for

the transport of local dust to the TALDICE site, since those trajectories passing over the Ross Sea became relatively more frequent. As a consequence, dust and nssCa$^{2+}$ fluxes in TALDICE are expected to decrease as it is indeed observed in both records. In addition, simultaneously elevated sea salt aerosol input would be expected due to an increased frequency of air masses passing over the Ross Sea. And indeed, looking at Fig. 4 it becomes evident that the decrease in J(nssCa$^{2+}$) after 8 ka BP is coeval with a significant increase in J(ssNa$^{+}$) in the TALDICE record. In fact, the fluxes of nssCa$^{2+}$ and ssNa$^{+}$ show a strongly anticorrelated behavior during the early Holocene. While both fluxes start decreasing at ≈ 18 ka BP, J(nssCa$^{2+}$) increases again after 12 ka BP to reach a local maximum at about 8 ka BP (upper panel in Fig. 4). J(ssNa$^{+}$) on the other hand is continuously decreasing until it reaches a local minimum at around 8 ka BP (lower panel in Fig. 4). This indicates that indeed air mass provenance is mainly responsible for Holocene dust and sea salt aerosol input changes at TALDICE, in addition to new local dust sources available during warm periods. In summary, based on our J(ssNa$^{+}$) and J(nssCa$^{2+}$) records we can corroborate the findings of Albani et al. (2012a) suggesting that more frequent air mass trajectories through the Ross Sea after 8 ka are mainly responsible for a reduced dust input from local sources after the Holocene maximum around 8 ka BP.

#### 3.1.2 Holocene versus MIS 5.5 ssNa$^{+}$ flux

When comparing J(ssNa$^{+}$) of the Holocene with marine isotope stage (MIS) 5.5 it becomes evident that the same level is reached in TALDICE for both interglacials, while for EDC and EDML fluxes during MIS 5.5 were only half (EDC) or even less (EDML) of the Holocene levels (see Fig. 3). EDC ssNa$^{+}$ flux is strongly related to winter sea ice extent in the Indian Ocean sector of the SO (Wolff et al., 2006) due to very low summer sea ice extent in this area even during glacial periods (Gersonde et al., 2005). However, EDML J(ssNa$^{+}$) during MIS 5.5 is even more reduced than in EDC possibly due to an even stronger decline in sea ice coverage in the Atlantic sector related to a reduction of both winter and summer sea extent in the Atlantic sector (Gersonde et al.,



2005; Fischer et al., 2007a). The very low ssNa$^{+}$ fluxes of EDC and EDML are in line with warmer Antarctic temperatures during MIS 5.5 compared to the Holocene (EPICA, 2006), causing significantly lower sea ice extent during that period. However, TALDICE J(ssNa$^{+}$) is at about the same level during both interglacial periods. This indicates that a substantial part of the ssNa$^{+}$ source regions for Talos Dome remains active during MIS 5.5, which excludes the Indian Ocean sector as a major ssNa$^{+}$ source region for Talos Dome, because this is the main source region for EDC where a drastic reduction of ssNa$^{+}$ input can be observed. Based on these observations we suggest that a major part of aerosol input to Talos Dome is originating from the Ross Sea sector not only during the Holocene but also during MIS 5.5. This consequently implies that a significant part of the sea ice cover in the Ross Sea embayment was persistent also during MIS 5.5 and was an active source for Talos Dome ssNa$^{+}$ input. This may be also of glaciological interest because the existence and/or extension of the Ross Ice Shelf during the warm MIS 5.5 period is controversial up to now (e.g. McKay et al., 2012).

#### 3.1.3 SsNa$^{+}$ flux during the last glacial period

During cold periods sea salt flux is rather constant compared to coeval ice extent changes inferred from marine sediment data. The sea salt flux in ice cores appears to be increasingly insensitive for very large sea ice extents as a result of the vast source area available when the sea ice around Antarctica extends further north. Additionally, the distance from the sea ice margin to the drill sites on the ice sheet is increasing and thus the travel time from the source to the deposition area is increasing significantly compared to the atmospheric lifetime of sea salt aerosol (Fischer et al., 2007b; Röthlisberger et al., 2010; Abram et al., 2013). Thus, during cold periods J(ssNa$^{+}$) in ice cores provides a tool for qualitative investigations on sea ice extent, however, quantitative interpretations are limited due to this effect.

In the period 115–20 ka BP TALDICE J(ssNa$^{+}$) is mostly lower than in EDML (bottom panel in Fig. 3). Only during two periods, each about ten thousand years long (40–30 ka BP and 65–55 ka BP, respectively), the sea salt aerosol input is higher in

TALDICE. The period 40–30 ka BP, including Antarctic Isotope Maxima (AIM) 8–4, is accompanied by a coeval higher signal in $\delta^{18}O$ in EDML relative to TALDICE (see Fig. 3, top panel), which indicates moderately elevated temperatures in the Atlantic sector possibly causing a decrease in sea ice extent in this region with a consequent impact on the $ssNa^+$ signal in EDML. Remarkably, EDML J($ssNa^+$) in this period is the lowest observed during the entire last glacial period. During the other period, 65–55 ka BP, marking the transition from MIS 4 into MIS 3, it was rather high TALDICE values instead of particularly low EDML values responsible for the inversion of the flux relationship. This high sea salt aerosol input in TALDICE is accompanied by large flux variations and marks a transition from low/moderate J($ssNa^+$) during MIS 5.4–MIS 4 (115–60 ka BP) to high fluxes during MIS 3 (60–25 ka BP); in fact the mean flux is increasing by a factor of 1.5. In contrast to Talos Dome such a shift in the mean $ssNa^+$ fluxes can be observed neither in EDC nor in EDML. There are indeed some distinct long term J($ssNa^+$) changes in both records, however, the variations remain around the same mean values for the entire last glacial period. Accordingly, the TALDICE record points to a shift in sea ice coverage in the Ross Sea sector from MIS 5 to MIS 3, which appears to be not so pronounced in the Atlantic or Indian Ocean sector as reflected in the EDML and EDC core, respectively. In contrast, at those two sites, a stronger shift in sea ice coverage is indicated during full interglacials compared to TALDICE, with the warmer MIS 5.5 showing even a substantially smaller sea ice extent compared to the Holocene.

### 3.2 Comparison of East Antarctic $nssCa^{2+}$ fluxes

It is evident that during glacial conditions J($nssCa^{2+}$) in all four ice cores are strongly related to temperature, albeit not linearly (see Fig. 3, note logarithmic axis for $nssCa^{2+}$). In particular it can be seen that J($nssCa^{2+}$) decrease significantly during each of the major AIM (EPICA, 2006), suggesting synchronous changes in the SSA source regions during warmer climate conditions of the last glacial (Wolff et al., 2006). It can also be



observed that J($nssCa^{2+}$) of EDC shows a very constant offset to EDML throughout the entire period shown in Fig. 3.

Only during AIM 8 (approx. 40 ka BP) EDC J($nssCa^{2+}$) shows a distinct dip with values reaching down to low interglacial level. These extreme low values are reached neither in the EDML nor in the TALDICE nor in the Vostok data during AIM 8. Even in the EDC record of insoluble dust particles (Lambert et al., 2008), which is otherwise strongly correlated to $nssCa^{2+}$, the AIM 8 minimum is not as pronounced as in the $nssCa^{2+}$ record, nor is it in the EDC $nssCa^{2+}$ data measured by ion chromatography (Wolff et al., 2006). Bigler et al. (2010) mentioned some distorted CFA $Ca^{2+}$ measurements due to occasional baseline fluctuations in the depth interval 585–788 m, comprising particularly AIM 8. Thus, EDC $nssCa^{2+}$ CFA data in the age interval 37.6–39 ka BP appear to be affected by analytical issues and are not included in further comparisons and are marked specifically in Fig. 6 (see figure caption for details).

As a consequence of the refusal of the extreme low EDC J($nssCa^{2+}$) values during AIM 8 we briefly revise the effects of Aeolian dust deposition in the Southern Ocean (and thus iron fertilisation) to atmospheric $CO_2$ changes as has been done by Röthlisberger et al. (2004). Based on our new data which allow for the calculation of an East Antarctic composite $nssCa^{2+}$ flux record we conclude that the upper limit of 20 ppm contribution of changes of iron supply to the SO to the total increase of 80–100 ppm $CO_2$ during the Last Glacial termination (T1) as suggested by Röthlisberger et al. (2004) is too low. Their calculations are relying strongly on the low $nssCa^{2+}$ flux during AIM 8 in EDC, which biases their regression and thus the estimated influence of reduced iron fertilisation to $CO_2$ increase significantly. Based on iron (Fe) records of EDC and Talos Dome, Vallelonga et al. (2013) estimated the impact of iron fertilisation through additional Fe input to the SO during the transition from MIS 3 into the LGM on atmospheric $CO_2$ to be in the order of 20 ppm. However, this is an estimate restricted to MIS 3/LGM only and thus, this value cannot be directly compared to the influence of iron fertilisation on the atmospheric $CO_2$ increase during T1 as discussed here. However, there have been other studies based on ice core Fe measurements investigating

T1 (Gaspari et al., 2006; Spolaor et al., 2013) which conclude that a reduction in iron fertilisation in the SO contributed to up to 40 ppm $CO_2$ increase during T1. Our composite nss$Ca^{2+}$ flux record from EDC, EDML, and TALDICE, respectively, was calculated as an arithmetic average, however with some special cases described in the following. EDML values were normalised with respect to EDC values in order not to bias the calculated mean. TALDICE values younger than 15 ka BP were discarded for the calculation because of their higher Holocene values compared to EDC and EDML due to the substantial contribution of local sources. During AIM 8 (A1), i.e. 39.3–37.4 ka BP, the EDC values were discarded (see Fig. 5a). In Fig. 5b the linear regressions of the composite J(nss$Ca^{2+}$) vs. atmospheric $CO_2$ are shown for T1 and for the period covering A1–A4, respectively, as done by Röthlisberger et al. (2004). Only due to the omission of the low EDC nss$Ca^{2+}$ flux during AIM 8, our regression through the points covering A1–A4 is much steeper compared to the one obtained by Röthlisberger et al. (2004). Following the argumentation of Röthlisberger et al. (2004) we conclude that the reduction of iron supply through reduced Aeolian dust deposition over the SO may have contributed up to 40 ppm to the atmospheric $CO_2$ increase during T1, which is in line with the results based on ice core Fe analyses of Gaspari et al. (2006).

While J(nss$Ca^{2+}$) of EDC and EDML evolved synchronously during the past 150 ka with a constant offset, TALDICE J(nss$Ca^{2+}$) values seem to oscillate between the other two records. Interestingly, TALDICE values are following the EDC fluxes during cold periods, while during warmer periods (grey shaded panels in Fig. 3) they are considerably higher than in EDC. This observation is discussed in Sect. 3.2.2. In the following section J(nss$Ca^{2+}$) of EDC and EDML are compared in more detail.

### 3.2.1 EDC versus EDML

Assuming a simple model of atmospheric aerosol transport as described by Fischer et al. (2007a) with an aerosol concentration $C_{\mathrm{air}}(0)$ at the source and an exponential loss during transport, the concentration of the aerosol in the air parcel at any time $t$ can be described as



$$C_{\mathrm{air}}(t) = C_{\mathrm{air}}(0) \cdot \exp(-t/\tau),$$

where $\tau$ is the average atmospheric residence time of the aerosol. Using this simple transport model and assuming a single source region (e.g. SSA), the logarithmic air concentration of the aerosol at one site (e.g. EDC) with transport time $t_2$ from the source location to the site can be expressed by the concentration at the same time of another site (e.g. EDML) with transport time $t_1$ according to

$$\ln\left[C_{\mathrm{air}}(t_2)\right] = \ln\left[C_{\mathrm{air}}(t_1)\right] - \Delta t/\tau,$$

where $\Delta t = t_2 - t_1$ is the difference of the transport times from the source to the two sites, assuming that the atmospheric residence time along the two transport ways is similar. Thus the relation of the logarithms of the atmospheric aerosol concentration at the two drilling sites is linear to first order with an offset $\Delta t/\tau$.

In Fig. 6 the logarithms of J(nss$Ca^{2+}$) and J(ss$Na^{+}$), respectively, are plotted for all three ice cores versus each other. In the first panel of Fig. 6a fluxes of EDC are plotted versus those of EDML, as it has been done previously by Fischer et al. (2007a) with the only difference that we use CFA data. In contrast, Fischer et al. (2007a) analysed the EDML ice core samples by IC with a significant blank contribution in the $Ca^{2+}$ data leading to a biased offset during warm (low concentration) periods. To illustrate this problem we plotted the EDML data analysed by IC versus EDC data in Fig. 6f with the only difference compared to Fischer et al. (2007a) that we used the AICC2012 age scale with its respective accumulation rate. In light green, all data are shown, in dark green the data with original $Ca^{2+}$ concentrations higher than 7 ppb, assuming that only data below this threshold are significantly biased by the blank contribution. A subsequent comparison of the linear regressions through all the IC data (slope $a$ of the regression is 1.26) and those above the threshold only ($a$ = 1.13) show that the IC data set is indeed approaching the slope of the CFA data set ($a$ = 1.02) when low concentration IC values are excluded. This procedure does not exclude the contaminated $Ca^{2+}$

data which exceed the threshold of 7 ppb and is therefore not providing a thorough correction, nevertheless, it is seen that the IC blank contribution has a significant effect which biases the outcome of the investigations as already mentioned in Fischer et al. (2007a). Furthermore, if data of the cold periods only is investigated, the two data sets (IC and CFA nssCa$^{2+}$) are in accordance with each other, resulting in the same linear regressions of the two plots (not shown).

When using CFA data only it can be seen that the offset $\Delta t/\tau$ has been constant over the whole period, the linear fit through all data points reveals a slope of $a = 1.02$ with a correlation coefficient of $r^2 = 0.87$ (total number of data points $N = 1336$). The offset $\Delta t/\tau$ during the Holocene is $1.22 \pm 0.65$, during the LGM is it $1.19 \pm 0.16$, thus virtually the same. This is remarkable since different glacial/interglacial variations in dust and other aerosol input have often been attributed to changes in wind speed and atmospheric circulation around Antarctica, and thus to transport effects (e.g. Petit et al., 1990, 1999). Indeed there have been more recent studies which suggest only moderate glacial/interglacial variations in wind speed and latitudinal shifts of the westerlies based on atmospheric circulation models (Krinner and Genthon, 1998, 2003; Mahowald et al., 2006; Sime et al., 2013), as well as based on size distribution of dust in East Antarctic ice cores (Delmonte et al., 2004). Based on our simple transport model we cannot see any transport effects influencing atmospheric dust concentrations at the two drilling sites during the last 150 ka. Yet, changing wind speeds (i.e. more efficient transport for colder climate conditions) could still be compensated by simultaneous changes of $\tau$. However, this would require decreased atmospheric residence times during colder periods, though $\tau$ is supposed to be longer during colder conditions (Yung et al., 1996; Petit et al., 1999; Lambert et al., 2008; Albani et al., 2012b). In summary, based on our multi-site J(nssCa$^{2+}$) records we conclude that transport intensity as well as atmospheric residence time plays a negligible role for the observed dust flux changes on the East Antarctic plateau during the last two glacial/interglacial cycles. Instead, our transport model suggests source strength changes to be mainly responsible for the pronounced J(nssCa$^{2+}$) changes (EDC and EDML nssCa$^{2+}$ flux ratio LGM/Holocene



$\approx 18$, see Table 1) on the East Antarctic plateau as it has been suggested by other studies before (e.g. Wolff et al., 2006; Fischer et al., 2007a).

Southern South America is believed to be the most important source region for glacial terrestrial aerosols to East Antarctica (Basile et al., 1997; Gaiero, 2007; Delmonte et al., 2008), whereas during warmer periods also Australia or other remote source regions might contribute to dust input in Antarctica (Revel-Rolland et al., 2006; Li et al., 2008; Marino et al., 2009; Gabrielli et al., 2010; Albani et al., 2012b). Based on the transport model applied in our study several source regions with considerable geographic distance can indeed not be excluded, however this would require similar $\Delta t/\tau$ values for all contributing sources or a constant source mix with different $\Delta t/\tau$ over time for each contributing source to obtain a linear relation between EDC and EDML J(nssCa$^{2+}$) as shown in Fig. 6a. Nevertheless, the variability of nssCa$^{2+}$ fluxes increases slightly for lower concentrations (Fig. 6a), thus for warmer climate conditions, which might be attributed to higher transport variability or additional dust input e.g. from Australia during warmer periods as mentioned above and discussed from a climate model point-of-view in Sect. 3.2.3.

The atmospheric lifetime $\tau$ of dust particles has been modelled to be in the order of 3–10 days by previous studies with no significant changes over glacial/interglacial changes (e.g. Yung et al., 1996; Mahowald et al., 1999; Werner et al., 2002; Tegen, 2003). The transport time for aerosol from the Atlantic sector of the East Antarctic ice sheet (EDML) to the EDC and TALDICE drilling sites according to the results of our transport model is in the range of 1.2–1.5 times the atmospheric life time. This results in a transportation time of about 4–15 days in line with back trajectory studies (Reijmer et al., 2002; Scarchilli et al., 2011). In Table 1 we compiled $\Delta t/\tau$ between EDML and EDC for the major climate periods over the last 150 ka. Interestingly, the largest change in $\Delta t/\tau$ cannot been found during T1 as it had been the case e.g. in Fischer et al. (2007a), but it gradually decreases through time since the last interglacial period (see Table 1). However, it has to be acknowledged that these changes reported in Table 1 are small compared to the given standard deviation. Nevertheless, based on our ice

core data we conclude that changes in transport and $\tau$ of aerosols are not subject to strong changes and change only slowly on millennial time scales. Instead, fast source strength changes seem to be mainly responsible for the rapid changes in the dust input to the East Antarctic plateau. This is also in line with processes as described e.g. by Sugden et al. (2009), where potential dust mobilization is coupled to glacial melt water deposition onto outwash plains in Patagonia. Other important parameters which govern continental aerosol source strength are surface wind speed, aridity, vegetation cover and weathering. Most of those are fast reacting parameters compared to millennial time scale changes and thus corroborate the hypothesis of source strength changes being mainly responsible for rapid changes in dust input on the East Antarctic ice sheet.

#### 3.2.2 TALDICE versus EDML, EDC, and Vostok

In contrast to the EDC/EDML comparison the good linear relationship between the logarithms of the nss$Ca^{2+}$ fluxes breaks down for TALDICE (Fig. 6c). Especially for lower concentrations, i.e. warmer conditions, there is a bias towards higher values in TALDICE. For this reason we divided the data in two groups, one for warm climate conditions the other for cold climate conditions. As a threshold between the two groups an arbitrary value of −38.9 ‰ of the $\delta^{18}$O TALDICE record has been chosen (dashed line in the top panel of Fig. 3). In Fig. 6d the data shown in Fig. 6c are discriminated by this $\delta^{18}$O threshold, resulting in two completely different regimes. While for cold climate conditions a linear relation between TALDICE and EDC exists (correlation coefficient of $r^2 = 0.75$, total number of data points $N = 728$), the two nss$Ca^{2+}$ fluxes are completely uncorrelated ($r^2 = 0.02$, $N = 588$) during warm periods. A similar behaviour can be observed when comparing TALDICE and EDML with strongly correlated J(nss$Ca^{2+}$) during cold periods ($r^2 = 0.77$, $N = 759$) and no correlation during warm periods ($r^2 = 5 \times 10^{-6}$, $N = 582$) (see Fig. 6b).

Furthermore, the offset $\Delta t/\tau$ is close to zero for glacial conditions of TALDICE vs. EDC (Fig. 6d) indicating that the transport times to both drilling sites are almost equal (assuming the same $\tau$ for both transport paths as well as the same source



region). The same observation is valid for the comparison of EDC with Vostok (see Fig. 6e) for the entire past 150 ka. However, it has to be considered that the Vostok data have been analysed with IC and show the same significant blank contribution for low $Ca^{2+}$ concentrations as the IC data of EDML, resulting in a bias towards higher values in the Vostok data for low values (see Fig. 6e).

An offset $\Delta t/\tau$ close to zero for EDC vs. TALDICE as well as Vostok, respectively, is in agreement with studies based on back trajectories which simulate the provenience of air parcels (Reijmer et al., 2002; Scarchilli et al., 2011) mostly originating from western pathways (dominated by the distinct Westerlies over the SO). However, recent simulations based on modern time meteorological data suggest that a significant part of air masses to Northern Victoria Land (i.e. Talos Dome) originate from atypical pathways, i.e. southern and eastern pathways instead of the common western pathways (Scarchilli et al., 2011; Delmonte et al., 2013). Albani et al. (2012a) attributed the changes of regional atmospheric transport patterns in the Victoria Land/Ross Sea embayment to the retreat of the Ross ice shelf during the early Holocene.

Higher J(nss$Ca^{2+}$) in TALDICE for warm climate conditions might also be explained by one or more additional dust sources which are only relevant for Northern Victoria Land, but not for the East Antarctic plateau. Previous studies on the isotopic signature ($^{87}Sr/^{86}Sr$ and $\epsilon_{Nd}(0)$) of interglacial dust from plateau ice cores show matching characteristics with dust from the Antarctic Dry Valleys (ADV) (Delmonte et al., 2007). More recent studies of the isotopic signatures of dust particles in TALDICE on the other hand show good agreement also with dust samples taken from the Mesa Range, Nunataks at the margin of the Antarctic plateau and close to Talos Dome (Delmonte et al., 2010a,b, 2013). However, the identification of a local sub-region by isotopic signature analyses of potential source areas is complicated due to the ubiquitous mixing of the TALDICE dust samples with volcanic particles (Delmonte et al., 2013).

While the geographical proximity and altitude favours the contribution of the Mesa Range, the source strength of the ADV is much enhanced during warm periods by glacial drift left behind from retreating glaciers, fluvial erosion and frost weathering due

to temperatures above 0 °C during the Antarctic summer. Furthermore, the ice-free area of the ADV was substantially smaller or even completely covered by ice sheets during the last glacial period (Denton and Hughes, 2002; Huybrechts, 2002), which reduces the source strength drastically during these periods. As shown by Hall and Denton (2000) the Ross Sea was not only covered by an ice shelf during the LGM as it is today, but there was the Ross Sea Ice Sheet reaching down from the ground of the Ross Sea up into the Dry Valleys with an altitude of up to 350 m a.s.l. Johnson et al. (2008) have shown that the Cape Adare region (at the north eastern edge of Northern Victoria land) was completely ice covered during the LGM and only became uncovered of ice at the transition into the Holocene at approx. 16 ka BP. In contrast, the Mesa Range was not covered by ice for the last 2 Myr as reconstructed by Oberholzer et al. (2008) by dating of moraines and erratic blocs with cosmogenic nuclides, involving a more constant source strength of the Mesa Range over glacial/interglacial and stadial/interstadial cycles. It can also be assumed that the dust source of the Mesa Range is depleted due to its long (uncovered) exposition to the atmosphere leading to a limited availability of mobile dust. Thus, we conclude that both proximal regions (ADV and Mesa Range) are potential local source regions for dust input to Talos Dome and dedicated tracer studies are needed to provide the final answer. Nevertheless, we suggest the ADV to be an efficient local dust source during the Holocene.

#### 3.2.3 Verification of our transport model by climate model data

In order to verify our transport model we consider climate model simulations described in Albani et al. (2012b) and Mahowald et al. (2006). The model output fields allow to plot the modelled dust deposition at EDML, EDC, Vostok, and TALDICE, respectively, the same way as done for ice core data discussed here, i.e. as double-logarithmic scatter plots for different ice core sites pairs as illustrated in Figs. 6 and 7. In addition knowing the source emissions in the model allows exploring the source-transport-deposition relations in a consistent framework. Our model allows for investigating equilibrium sim-



ulations from two climate periods, i.e. current climate (representative of the Holocene) and the LGM.

Because for the exponential transport model we considered the flux of ice core aerosol data representative for the atmospheric aerosol concentration at the drill site (see Sect. 2.3), we consider both modelled dust deposition flux and dust load at corresponding ice core locations. Figure 7a shows the average atmospheric dust load from two 1 yr simulations (one simulation for Holocene and one for LGM climate). A very similar behaviour can be observed when comparing the model results in Fig. 7a with the ice core data in Fig. 6. EDC, Vostok, and TALDICE model data show slopes of $\approx 1$, with EDC and Vostok exhibiting a very small $\Delta t/\tau$ offset, thus the regression line lying almost on the 1 : 1 slope. Higher dust loadings for TALDICE and in particular for EDML (due to its proximity to the main source areas in SSA) result in a distinct offset compared to EDC and Vostok, respectively, for both climate periods as observed in the ice core data as well at least for EDML. In addition, the slope of EDML shows a slightly higher value. If we now consider dust deposition instead of atmospheric surface concentration of the very same model run (Fig. 7b), we see all the regression lines having slopes close to 1, but more distinct offsets. The uncertainty is unconstrained, as we are just using 2 points (average for current climate and LGM). Nonetheless, we infer that the slopes are representative of the modelled relations based on a set of longer (10 yr data at the equilibrium) simulations with the same model (Mahowald et al., 2006). The only difference is that the emissions rates from Australia were tuned (half in the current climate and double in the LGM) in the 1 yr simulations to better match the observed dust fluxes and source apportionment (Albani et al., 2012b). This results in slightly more scattered slopes for both dust loading (Fig. 7c) and deposition flux (Fig. 7d), but allows for an estimation of the error and $r^2$ of the regression lines (in Table 2 the slopes, standard deviations, and $r^2$ values for all regressions shown in Fig. 7 are indicated).

Note that even for the 10 yr simulations, the linear regression in Fig. 7c and d is defined by two clouds of points representative for the climate and accumulation extremes during the Holocene and LGM, respectively. In contrast, the ice core data in Fig. 6 cover

the whole spectrum of dust conditions from the glacial maximum to the Holocene, covering the long glaciations as well as the glacial/interglacial transition. This implies that the influence of the Holocene, characterized by the highest precipitation rates, on the regression line is much smaller in the ice core data, as it represents only about a tenth of all data points used in the regression, while it represents 50 % of the data points defining the regression lines in Fig. 7. This effect may be partly responsible for the difference in the slope between data and model for EDML. Based on the overall good correspondence of the slopes in the regression lines for atmospheric dust loadings in Fig. 7a and c, we conclude that our transport model appears to be able to describe the transport effect on dust concentrations in different regions on the East Antarctic ice sheet.

The differences between modelled dust loading and deposition (compare Fig. 7a/c with b/d) reflect the deposition processes in the model. For our exponential-decay transport model applied on the ice core flux data we assume dry deposition only (see Sect. 2.3), which is a reasonable approximation for interior sites such as EDC and Vostok (Wolff et al., 2006) and for all sites in the glacial, where snow accumulation was about 50 % lower than today, but may be inadequate in the case of peripheral sites such as EDML and Talos Dome for recent accumulation rate conditions. On the other hand the Mahowald et al. (2006) model simulates both dry and wet deposition, in proportions that are well represented for coastal Antarctic sites, but likely overestimate the contribution of wet deposition on the plateau (Albani et al., 2012b), thus leading to much larger differences in the logarithmic deposition fluxes in EDML and Talos Dome relative to EDC than in the modelled atmospheric concentrations.

A comparison of the ice core data $\Delta t/\tau$ offsets reported in Table 1 and shown in Fig. 6 with modelled ones (Fig. 7b and d) shows that the modelled deposition is biased highly for TALDICE and EDML, possibly in relation to too high simulated snow precipitation rates (Albani et al., 2012b). However, since the glacial/interglacial increase in snow deposition of a factor 2 is well captured by the model (Albani et al., 2012b), the slope of $\sim 1$ is well reproduced, so there is a solid base to discuss the model results in com-



parison with the observations and making inferences on the underlying mechanisms, based on model physics.

With the model we can also explore the relation between source emissions from a specific area to the dust deposition. Considering (logarithmic transforms of) emissions and dust deposition from South America alone (Fig. 7e) gives a slope of $\sim 1$ between emission and deposition for all ice cores. The only exception is TALDICE, which has a major Australian contribution in the model. This result is not surprising considering that the source experiencing the largest changes in modelled emissions is South America, with a factor of 13 compared to a factor of 4 of Australia (Albani et al., 2012b). In addition, its relative abundance for modelled dust deposition at ice core sites is either dominant (EDML) or increasing in the LGM for the other sites. So it is not surprising that it is driving the slope, and may be the reason why the approximation of a unique source implicit in the exponential transport model holds in reproducing the $\sim 1$ slope, despite the observed complexity of the dust provenance mix especially in the Holocene (see Introduction). The reason why the logarithms of TALDICE vs. EDC dust deposition in the model show a slope of $\sim 1$ at all, which is not consistent with the ice core data due to the strong contribution of local sources at Talos Dome during the Holocene (see Sect. 3.2.2), is because the model does not consider local (Antarctic) sources, and thus, this particular observations in Talos Dome ice core data cannot be captured in the model.

The question remains whether constant transport efficiency (i.e. constant $\Delta t/\tau$) represents a unique solution to explain the regression lines in Fig. 6, or whether changes in the source mix may also allow for a slope 1 relationship between different ice core sites in Antarctica. Interestingly, the Mahowald et al. (2006) model actually simulates a decrease in dust lifetimes ($\tau$) in the glacial, which would increase the slope in Fig. 7, if transport times would stay constant. At the same time transport efficiency in the model is increased from both Australia and South America in the glacial, which for the latter means a more focused/direct transport, possibly indicating shorter transport times. Overall the deposition efficiency, which summarizes the mentioned changes in trans-

port and lifetimes, tends to increase for the sites of interest, but at different rates and with spatial patterns depending on the source (Figs. 8 and 9 in Albani et al., 2012b). In conclusion the model described in Albani et al. (2012b) would support only partly balancing effects in dust lifetimes and transport time on dust exported from southern South America. This would tend to support the idea that the slope 1 relation is also consistent with a more complex scenario involving changes in source emissions in the first place, mediated by the changing proportions of dust contributions to ice core sites and parallel changes in transport and residence time of dust. Uncertainties still exist in modelled dust fluxes, as the model is still not able to quantitatively fully reproduce the glacial/interglacial deposition fluxes for all the ice cores in Antarctica (Albani et al., 2012b). Future improved model studies will help to better disentangle the source and transport contributions to glacial/interglacial dust changes in Antarctica.

## 4 Conclusions

In this study we presented new CFA nss$Ca^{2+}$ and ss$Na^{+}$ records of the Talos Dome ice core in centennial resolution reaching back 150 ka BP. TALDICE nss$Ca^{2+}$ flux shows both large-scale changes on glacial/interglacial time scales as well as a regional signal, emerging when dust advection from remote sources was extremely low, i.e. during warm (interglacial) periods. Dust deposition at Talos Dome reflects major climate changes on a hemispheric scale during the last 150 ka. However, the significant contribution of proximal dust sources during warm climate periods (e.g. the Holocene) makes Talos Dome sensitive to regional atmospheric circulation changes. Our new nss$Ca^{2+}$ and ss$Na^{+}$ flux records corroborate the scenario proposed by Albani et al. (2012a) suggesting that more frequent air mass trajectories through the Ross Sea are mainly responsible for a reduced dust input from local sources after 8 ka BP. Since there are no TALDICE nss$Ca^{2+}$ and ss$Na^{+}$ data available for the late Holocene, we cannot examine the behaviour of the two parameters in the context of a late Holocene Ross Ice Shelf re-advance (Albani et al., 2012a). An extension of the existing records to the last three



millennia would allow for a verification of an according behaviour. Nevertheless, based on the new TALDICE aerosol records we suggest similar regional climate conditions as observed during the Holocene prevailing also during the past interglacial period in the Ross Sea area. In particular, our new J(ss$Na^{+}$) data indicate the presence of extended sea ice cover in the Ross Sea area during MIS 5.5 of similar extent as during the Holocene.

Two potential local source regions, which could not been discriminated unambiguously as main contributors to local dust input to Talos Dome so far, may contribute to the higher dust fluxes during warm periods, the Antarctic Dry Valleys and/or the Mesa Range (Delmonte et al., 2013). The Dry Valleys are considered to be an efficient dust source because glacial drift deposits, fluvial erosion, and frost weathering enhance the availability of mobile dust during warm periods, while during cold periods this source region is ice covered and thus no longer active, which is in line with our new TALDICE nss$Ca^{2+}$ data.

The availability of three highly resolved J(nss$Ca^{2+}$) records (EDC, EDML, and TALDICE, respectively) allow for a revision of the estimate on atmospheric $CO_2$ sensitivity to dust induced iron fertilisation in the Southern Ocean. Röthlisberger et al. (2004) based their estimation on the only record available at that time (CFA nss$Ca^{2+}$ of EDC) including extremely low values during AIM 8 which, however, have not been observed in other ice core records. Accordingly, their finding of 20 ppm seems to underestimate the $CO_2$ sensitivity. In a revised estimation, including J(nss$Ca^{2+}$) of TALDICE, EDML, and EDC and discarding the extreme low EDC values during AIM 8, we estimate the increase of atmospheric $CO_2$ during T1 linked to reduced dust induced iron fertilisation in the SO to be up to 40 ppm.

Based on our exponential transport model applied on nss$Ca^{2+}$ records of four East Antarctic ice cores we cannot see any long range transport effects influencing atmospheric dust concentration changes in East Antarctica. While a comparison with climate model results confirm our findings of constant offsets in $\Delta t/\tau$ for dust fluxes at the four drill sites for Holocene/LGM climate, the model supports the concept that the slope

$\sim 1$ relation would be also consistent with a more complex scenario involving changes in source emissions in the first place, mediated by the changing proportions of dust contributions to ice core sites and changes in transport and residence time of dust. We conclude that the observed nss$Ca^{2+}$ flux changes predominantly reflect changes in South America source strength during the past 150 ka. Changing transport time and atmospheric residence time may have contributed in determining the magnitude of the observed flux changes.

The transport time for aerosol from the Atlantic sector of the East Antarctic ice sheet (EDML) to the EDC and TALDICE drilling sites according to the results of our transport model is in the range of 1.2–1.5 times the atmospheric life time. Assuming a typical lifetime of 3–10 days, we get a transportation time of 4–15 days, with the largest transport times for the ice core sites furthest away from the glacial SSA source region.

*Acknowledgements.* We thank the AWI team, in particular Anna Wegner and Birthe Twarloh, as well as Patrik Kaufmann, Matthias Bigler, and Christof Bernhard for their support during the CFA analyses. This research is funded by the Swiss National Science Foundation and the Prince Albert II of Monaco foundation. The Talos Dome Ice core Project (TALDICE), a joint European programme, is funded by national contributions from Italy, France, Germany, Switzerland and the UK. Primary logistical support was provided by PNRA at Talos Dome. This is TALDICE publication no. 35.

## References

Abram, N. J., Wolff, E. W., and Curran, M. A. J.: A review of sea ice proxy information from polar ice cores, Quaternary Sci. Rev., doi:10.1016/j.quascirev.2013.01.011, 2013. 3324, 3326, 3334

Albani, S., Delmonte, B., Maggi, V., Baroni, C., Petit, J.-R., Stenni, B., Mazzola, C., and Frezzotti, M.: Interpreting last glacial to Holocene dust changes at Talos Dome (East Antarctica): implications for atmospheric variations from regional to hemispheric scales, Clim. Past, 8, 741–750, doi:10.5194/cp-8-741-2012, 2012a. 3325, 3332, 3333, 3342, 3347, 3364



Albani, S., Mahowald, N., Delmonte, B., Maggi, V., and Winckler, G.: Comparing modeled and observed changes in mineral dust transport and deposition to Antarctica between the Last Glacial Maximum and current climates, Clim. Dynam., 38, 1731–1755, doi:10.1007/s00382-011-1139-5, 2012b. 3339, 3340, 3343, 3344, 3345, 3346, 3347, 3370

Archer, D., Winguth, A., Lea, D., and Mahowald, N.: What caused the glacial/interglacial atmospheric $pCO_2$ cycles?, Rev. Geophys., 38, 159–189, doi:10.1029/1999rg000066, 2000. 3324

Basile, I., Grousset, F. E., Revel, M., Petit, J. R., Biscaye, P. E., and Barkov, N. I.: Patagonian origin of glacial dust deposited in East Antarctica (Vostok and Dome C) during glacial stages 2, 4 and 6, Earth Planet. Sc. Lett., 146, 573–589, doi:10.1016/S0012-821X(96)00255-5, 1997. 3325, 3340

Bazin, L., Landais, A., Lemieux-Dudon, B., Toyé Mahamadou Kele, H., Veres, D., Parrenin, F., Martinerie, P., Ritz, C., Capron, E., Lipenkov, V., Loutre, M.-F., Raynaud, D., Vinther, B., Svensson, A., Rasmussen, S. O., Severi, M., Blunier, T., Leuenberger, M., Fischer, H., Masson-Delmotte, V., Chappellaz, J., and Wolff, E.: An optimized multi-proxy, multi-site Antarctic ice and gas orbital chronology (AICC2012): 120–800 ka, Clim. Past Discuss., 8, 5963–6009, doi:10.5194/cpd-8-5963-2012, 2012. 3328, 3329, 3362

Bereiter, B., Lüthi, D., Siegrist, M., Schüpbach, S., Stocker, T. F., and Fischer, H.: Mode change of millennial $CO_2$ variability during the last glacial cycle associated with a bipolar marine carbon seesaw, P. Natl. Acad. Sci., 109, 9755–9760, doi:10.1073/pnas.1204069109, 2012. 3324, 3366

Bigler, M., Röthlisberger, R., Lambert, F., Stocker, T. F., and Wagenbach, D.: Aerosol deposited in East Antarctica over the last glacial cycle: Detailed apportionment of continental and sea-salt contributions, J. Geophys. Res., 111, D08205, doi:10.1029/2005JD006469, 2006. 3327, 3330, 3363

Bigler, M., Röthlisberger, R., Lambert, F., Wolff, E. W., Castellano, E., Udisti, R., Stocker, T. F., and Fischer, H.: Atmospheric decadal variability from high-resolution Dome C ice core records of aerosol constituents beyond the Last Interglacial, Quaternary Sci. Rev., 29, 324–337, doi:10.1016/j.quascirev.2009.09.009, 2010. 3324, 3327, 3336

Blunier, T., Schwander, J., Stauffer, B., Stocker, T., Dällenbach, A., Indermühle, A., Tschumi, J., Chappellaz, J., Raynaud, D., and Barnola, J. M.: Timing of the Antarctic Cold Reversal and the atmospheric $CO_2$ increase with respect to the Younger Dryas event, Geophys. Res. Lett., 24, 2683–2686, doi:10.1029/97GL02658, 1997. 3324

Bory, A., Wolff, E., Mulvaney, R., Jagoutz, E., Wegner, A., Ruth, U., and Elderfield, H.: Multiple sources supply eolian mineral dust to the Atlantic sector of coastal Antarctica: Evidence from recent snow layers at the top of Berkner Island ice sheet, Earth Planet. Sc. Lett., 291, 138–148, doi:10.1016/j.epsl.2010.01.006, 2010. 3325

Bouttes, N., Paillard, D., and Roche, D. M.: Impact of brine-induced stratification on the glacial carbon cycle, Clim. Past, 6, 575–589, doi:10.5194/cp-6-575-2010, 2010. 3324

Brook, E. J., White, J. W. C., Schilla, A. S. M., Bender, M. L., Barnett, B., Severinghaus, J. P., Taylor, K. C., Alley, R. B., and Steig, E. J.: Timing of millennial-scale climate change at Siple Dome, West Antarctica, during the last glacial period, Quaternary Sci. Rev., 24, 1333–1343, doi:10.1016/j.quascirev.2005.02.002, 2005. 3324

Buiron, D., Chappellaz, J., Stenni, B., Frezzotti, M., Baumgartner, M., Capron, E., Landais, A., Lemieux-Dudon, B., Masson-Delmotte, V., Montagnat, M., Parrenin, F., and Schilt, A.: TALDICE-1 age scale of the Talos Dome deep ice core, East Antarctica, Clim. Past, 7, 1–16, doi:10.5194/cp-7-1-2011, 2011. 3330

De Angelis, M., Steffensen, J. P., Legrand, M., Clausen, H., and Hammer, C.: Primary aerosol (sea salt and soil dust) deposited in Greenland ice during the last climatic cycle: Comparison with east Antarctic records, J. Geophys. Res.-Oceans, 102, 26681–26698, doi:10.1029/97jc01298, 1997. 3327, 3328, 3363

Delmonte, B., Petit, J. R., Basile-Doelsch, I., Jagoutz, E., and Maggi, V.: Developments in Quaternary Sciences, vol. 7, chap. 6: Late quaternary interglacials in East Antarctica from ice-core dust records, Elsevier, 53–73, 2007. 3342

Delmonte, B., Andersson, P. S., Hansson, M., Schöberg, H., Petit, J. R., Basile-Doelsch, I., and Maggi, V.: Aeolian dust in East Antarctica (EPICA-Dome C and Vostok): Provenance during glacial ages over the last 800 kyr, Geophys. Res. Lett., 35, L07703, doi:10.1029/2008GL033382, 2008. 3325, 3340

Delmonte, B., Andersson, P. S., Schöberg, H., Hansson, M., Petit, J. R., Delmas, R., Gaiero, D. M., Maggi, V., and Frezzotti, M.: Geographic provenance of aeolian dust in East Antarctica during Pleistocene glaciations: preliminary results from Talos Dome and comparison with East Antarctic and new Andean ice core data, Quaternary Sci. Rev., 29, 256–264, doi:10.1016/j.quascirev.2009.05.010, 2010a. 3342

Delmonte, B., Baroni, C., Andersson, P. S., Schöberg, H., Hansson, M., Aciego, S., Petit, J. R., Albani, S., Mazzola, C., Maggi, V., and Frezzotti, M.: Aeolian dust in the Talos Dome ice core (East Antarctica, Pacific/Ross Sea sector): Victoria Land versus remote sources over the last



two climate cycles, J. Quaternary Sci., 25, 1327–1337, doi:10.1002/jqs.1418, 2010b. 3325, 3342

Delmonte, B., Baroni, C., Andersson, P. S., Narcisi, B., Salvatore, M. C., Petit, J. R., Scarchilli, C., Frezzotti, M., Albani, S., and Maggi, V.: Modern and Holocene aeolian dust variability from Talos Dome (Northern Victoria Land) to the interior of the Antarctic ice sheet, Quaternary Sci. Rev., 64, 76–89, doi:10.1016/j.quascirev.2012.11.033, 2013. 3325, 3326, 3342, 3348

Denton, G. H. and Hughes, T. J.: Reconstructing the Antarctic Ice Sheet at the Last Glacial Maximum, Quaternary Sci. Rev., 21, 193–202, doi:10.1016/S0277-3791(01)00090-7, 2002. 3343

Dieckmann, G. S. and Hellmer, H. H.: The Importance of Sea Ice: An Overview, Wiley-Blackwell, 1–22, 2010. 3324

EPICA, C. M.: Eight glacial cycles from an Antarctic ice core, Nature, 429, 623–628, doi:10.1038/nature02599, 2004. 3324, 3326

EPICA, C. M.: One-to-one coupling of glacial climate variability in Greenland and Antarctica, Nature, 444, 195–198, doi:10.1038/nature05301, 2006. 3324, 3326, 3334, 3335, 3363

Fischer, H., Fundel, F., Ruth, U., Twarloh, B., Wegner, A., Udisti, R., Becagli, S., Castellano, E., Morganti, A., Severi, M., Wolff, E. W., Littot, G., Röthlisberger, R., Mulvaney, R., Hutterli, M. A., Kaufmann, P., Federer, U., Lambert, F., Bigler, M., Hansson, M., Jonsell, U., de Angelis, M., Boutron, C., Siggaard-Andersen, M.-L., Steffensen, J. P., Barbante, C., Gaspari, V., Gabrielli, P., and Wagenbach, D.: Reconstruction of millennial changes in dust emission, transport and regional sea ice coverage using the deep EPICA ice cores from the Atlantic and Indian Ocean sector of Antarctica, Earth Planet. Sc. Lett., 260, 340–354, doi:10.1016/j.epsl.2007.06.014, 2007a. 3326, 3327, 3328, 3334, 3337, 3338, 3339, 3340, 3368

Fischer, H., Siggaard-Andersen, M.-L., Ruth, U., Röthlisberger, R., and Wolff, E. W.: Glacial/interglacial changes in mineral dust and sea-salt records in polar ice cores: Sources, transport, and deposition, Rev. Geophys., 45, RG1002, doi:10.1029/2005RG000192, 2007b. 3324, 3326, 3330, 3331, 3334

Fischer, H., Schmitt, J., Lüthi, D., Stocker, T. F., Tschumi, T., Parekh, P., Joos, F., Köhler, P., Völker, C., Gersonde, R., Barbante, C., Le Floch, M., Raynaud, D., and Wolff, E.: The role of Southern Ocean processes in orbital and millennial $CO_2$ variations – A synthesis, Quaternary Sci. Rev., 29, 193–205, doi:10.1016/j.quascirev.2009.06.007, 2010. 3324

Frezzotti, M., Urbini, S., Proposito, M., Scarchilli, C., and Gandolfi, S.: Spatial and temporal variability of surface mass balance near Talos Dome, East Antarctica, J. Geophys. Res., 112, F02032, doi:10.1029/2006jf000638, 2007. 3325

Gabrielli, P., Wegner, A., Petit, J. R., Delmonte, B., De Deckker, P., Gaspari, V., Fischer, H., Ruth, U., Kriews, M., Boutron, C., Cescon, P., and Barbante, C.: A major glacial-interglacial change in aeolian dust composition inferred from Rare Earth Elements in Antarctic ice, Quaternary Sci. Rev., 29, 265–273, doi:10.1016/j.quascirev.2009.09.002, 2010. 3325, 3340

Gaiero, D. M.: Dust provenance in Antarctic ice during glacial periods: From where in southern South America?, Geophys. Res. Lett., 34, L17707, doi:10.1029/2007gl030520, 2007. 3325, 3340

Gaspari, V., Barbante, C., Cozzi, G., Cescon, P., Boutron, C. F., Gabrielli, P., Capodaglio, G., Ferrari, C., Petit, J. R., and Delmonte, B.: Atmospheric iron fluxes over the last deglaciation: Climatic implications, Geophys. Res. Lett., 33, L03704, doi:10.1029/2005gl024352, 2006. 3337

Gersonde, R., Crosta, X., Abelmann, A., and Armand, L.: Sea-surface temperature and sea ice distribution of the Southern Ocean at the EPILOG Last Glacial Maximum—a circum-Antarctic view based on siliceous microfossil records, Quaternary Sci. Rev., 24, 869–896, doi:10.1016/j.quascirev.2004.07.015, 2005. 3333

Hall, B. L. and Denton, G. H.: Extent and Chronology of the Ross Sea Ice Sheet and the Wilson Piedmont Glacier along the Scott Coast at and since the Last Glacial Maximum, Geogr. Ann. A, 82, 337–363, doi:10.1111/j.0435-3676.2000.00128.x, 2000. 3343

Huybrechts, P.: Sea-level changes at the LGM from ice-dynamic reconstructions of the Greenland and Antarctic ice sheets during the glacial cycles, Quaternary Sci. Rev., 21, 203–231, doi:10.1016/S0277-3791(01)00082-8, 2002. 3343

Johnson, J. S., Hillenbrand, C.-D., Smellie, J. L., and Rocchi, S.: The last deglaciation of Cape Adare, northern Victoria Land, Antarctica, Antarct. Sci., 20, 581–587, doi:10.1017/S0954102008001417, 2008. 3343

Jouzel, J., Masson-Delmotte, V., Cattani, O., Dreyfus, G., Falourd, S., Hoffmann, G., Minster, B., Nouet, J., Barnola, J. M., Chappellaz, J., Fischer, H., Gallet, J. C., Johnsen, S., Leuenberger, M., Loulergue, L., Lüthi, D., Oerter, H., Parrenin, F., Raisbeck, G., Raynaud, D., Schilt, A., Schwander, J., Selmo, E., Souchez, R., Spahni, R., Stauffer, B., Steffensen, J. P., Stenni, B., Stocker, T. F., Tison, J. L., Werner, M., and Wolff, E. W.: Orbital and Millennial Antarctic Climate Variability over the Past 800,000 Years, Science, 317, 793–796, doi:10.1126/science.1141038, 2007. 3324



Kaufmann, P. R., Federer, U., Hutterli, M. A., Bigler, M., Schüpbach, S., Ruth, U., Schmitt, J., and Stocker, T. F.: An Improved Continuous Flow Analysis System for High-Resolution Field Measurements on Ice Cores, Environ. Sci. Technol., 42, 8044–8050, doi:10.1021/es8007722, 2008. 3327, 3328

Kaufmann, P. R., Fundel, F., Fischer, H., Bigler, M., Ruth, U., Udisti, R., Hansson, M., de Angelis, M., Barbante, C., Wolff, E. W., Hutterli, M. A., and Wagenbach, D.: Ammonium and non-sea salt sulfate in the EPICA ice cores as indicator of biological activity in the Southern Ocean, Quaternary Sci. Rev., 29, 313–323, doi:10.1016/j.quascirev.2009.11.009, 2010. 3327, 3363

Knorr, G. and Lohmann, G.: Southern Ocean origin for the resumption of Atlantic thermohaline circulation during deglaciation, Nature, 424, 532–536, doi:10.1038/nature01855, 2003. 3324

Krinner, G. and Genthon, C.: GCM simulations of the Last Glacial Maximum surface climate of Greenland and Antarctica, Clim. Dynam., 14, 741–758, doi:10.1007/s003820050252, 1998. 3339

Krinner, G. and Genthon, C.: Tropospheric transport of continental tracers towards Antarctica under varying climatic conditions, Tellus B, 55, 54–70, doi:10.1034/j.1600-0889.2003.00004.x, 2003. 3339

Lambert, F., Delmonte, B., Petit, J. R., Bigler, M., Kaufmann, P. R., Hutterli, M. A., Stocker, T. F., Ruth, U., Steffensen, J. P., and Maggi, V.: Dust-climate couplings over the past 800,000 years from the EPICA Dome C ice core, Nature, 452, 616–619, doi:10.1038/nature06763, 2008. 3336, 3339

Li, F., Ginoux, P., and Ramaswamy, V.: Distribution, transport, and deposition of mineral dust in the Southern Ocean and Antarctica: Contribution of major sources, J. Geophys. Res. Atmos., 113, D10207, doi:10.1029/2007jd009190, 2008. 3325, 3340

Mahowald, N. M., Kohfeld, K., Hansson, M., Balkanski, Y., Harrison, S. P., Prentice, I. C., Schulz, M., and Rodhe, H.: Dust sources and deposition during the last glacial maximum and current climate: A comparison of model results with paleodata from ice cores and marine sediments, J. Geophys. Res.-Atmos., 104, 15895–15916, doi:10.1029/1999jd900084, 1999. 3340

Mahowald, N. M., Muhs, D. R., Levis, S., Rasch, P. J., Yoshioka, M., Zender, C. S., and Luo, C.: Change in atmospheric mineral aerosols in response to climate: Last glacial period, preindustrial, modern, and doubled carbon dioxide climates, J. Geophys. Res.-Atmos., 111, D10202, doi:10.1029/2005jd006653, 2006. 3339, 3343, 3344, 3345, 3346

Marino, F., Castellano, E., Nava, S., Chiari, M., Ruth, U., Wegner, A., Lucarelli, F., Udisti, R., Delmonte, B., and Maggi, V.: Coherent composition of glacial dust on opposite sides of the East Antarctic Plateau inferred from the deep EPICA ice cores, Geophys. Res. Lett., 36, L23703, doi:10.1029/2009gl040732, 2009. 3325, 3340

Martin, J. H.: Glacial-interglacial $CO_2$ change: The Iron Hypothesis, Paleoceanography, 5, 1–13, doi:10.1029/PA005i001p00001, 1990. 3324

McKay, R., Naish, T., Powell, R., Barrett, P., Scherer, R., Talarico, F., Kyle, P., Monien, D., Kuhn, G., Jackolski, C., and Williams, T.: Pleistocene variability of Antarctic Ice Sheet extent in the Ross Embayment, Quaternary Sci. Rev., 34, 93–112, doi:10.1016/j.quascirev.2011.12.012, 2012. 3334

Oberholzer, P., Baroni, C., Salvatore, M., Baur, H., and Wieler, R.: Dating late Cenozoic erosional surfaces in Victoria Land, Antarctica, with cosmogenic neon in pyroxenes, Antarct. Sci., 20, 89–98, doi:10.1017/S095410200700079X, 2008. 3343

Petit, J. R. and Delmonte, B.: A model for large glacial-interglacial climate-induced changes in dust and sea salt concentrations in deep ice cores (central Antarctica): palaeoclimatic implications and prospects for refining ice core chronologies, Tellus B, 61, 768–790, doi:10.1111/j.1600-0889.2009.00437.x, 2009. 3325, 3326

Petit, J. R., Mourner, L., Jouzel, J., Korotkevich, Y. S., Kotlyakov, V. I., and Lorius, C.: Palaeoclimatological and chronological implications of the Vostok core dust record, Nature, 343, 56–58, doi:10.1038/343056a0, 1990. 3324, 3339

Petit, J. R., Jouzel, J., Raynaud, D., Barkov, N. I., Barnola, J. M., Basile, I., Bender, M., Chappellaz, J., Davis, M., Delaygue, G., Delmotte, M., Kotlyakov, V. M., Legrand, M., Lipenkov, V. Y., Lorius, C., Pepin, L., Ritz, C., Saltzman, E., and Stievenard, M.: Climate and atmospheric history of the past 420,000 years from the Vostok ice core, Antarctica, Nature, 399, 429–436, doi:10.1038/20859, 1999. 3324, 3326, 3339

Rankin, A. M., Auld, V., and Wolff, E. W.: Frost flowers as a source of fractionated sea salt aerosol in the polar regions, Geophys. Res. Lett., 27, 3469–3472, doi:10.1029/2000gl011771, 2000. 3326

Reijmer, C. H., van den Broeke, M. R., and Scheele, M. P.: Air Parcel Trajectories and Snowfall Related to Five Deep Drilling Locations in Antarctica Based on the ERA-15 Dataset, J. Climate, 15, 1957–1968, doi:10.1175/1520-0442(2002)015<1957:APTASR>2.0.CO;2, 2002. 3326, 3340, 3342



Revel-Rolland, M., De Deckker, P., Delmonte, B., Hesse, P. P., Magee, J. W., Basile-Doelsch, I., Grousset, F., and Bosch, D.: Eastern Australia: A possible source of dust in East Antarctica interglacial ice, Earth Planet. Sc. Lett., 249, 1–13, doi:10.1016/j.epsl.2006.06.028, 2006. 3325, 3340

Röthlisberger, R., Bigler, M., Hutterli, M. A., Sommer, S., Stauffer, B., Junghans, H. G., and Wagenbach, D.: Technique for Continuous High-Resolution Analysis of Trace Substances in Firn and Ice Cores, Environ. Sci. Technol., 34, 338–342, doi:10.1021/es9907055, 2000. 3327, 3328

Röthlisberger, R., Mulvaney, R., Wolff, E. W., Hutterli, M. A., Bigler, M., Sommer, S., and Jouzel, J.: Dust and sea salt variability in central East Antarctica (Dome C) over the last 45 kyrs and its implications for southern high-latitude climate, Geophys. Res. Lett., 29, 1963, doi:10.1029/2002GL015186, 2002. 3324

Röthlisberger, R., Bigler, M., Wolff, E. W., Joos, F., Monnin, E., and Hutterli, M. A.: Ice core evidence for the extent of past atmospheric $CO_2$ change due to iron fertilisation, Geophys. Res. Lett., 31, L16207, doi:10.1029/2004GL020338, 2004. 3327, 3336, 3337, 3348, 3366

Röthlisberger, R., Crosta, X., Abram, N. J., Armand, L., and Wolff, E. W.: Potential and limitations of marine and ice core sea ice proxies: an example from the Indian Ocean sector, Quaternary Sci. Rev., 29, 296–302, doi:10.1016/j.quascirev.2009.10.005, 2010. 3326, 3334

Scarchilli, C., Frezzotti, M., and Ruti, P.: Snow precipitation at four ice core sites in East Antarctica: provenance, seasonality and blocking factors, Clim. Dynam., 37, 2107–2125, doi:10.1007/s00382-010-0946-4, 2011. 3326, 3340, 3342

Sime, L. C., Kohfeld, K. E., Le Quéré, C., Wolff, E. W., de Boer, A. M., Graham, R. M., and Bopp, L.: Southern Hemisphere westerly wind changes during the Last Glacial Maximum: model-data comparison, Quaternary Sci. Rev., 64, 104–120, doi:10.1016/j.quascirev.2012.12.008, 2013. 3339

Spolaor, A., Vallelonga, P., Cozzi, G., Gabrieli, J., Varin, C., Kehrwald, N., Zennaro, P., Boutron, C., and Barbante, C.: Iron speciation in aerosol dust influences iron bioavailability over glacial-interglacial timescales, Geophys. Res. Lett., 40, 1618–1623, doi:10.1002/grl.50296, 2013. 3337

Stenni, B., Buiron, D., Frezzotti, M., Albani, S., Barbante, C., Bard, E., Barnola, J. M., Baroni, M., Baumgartner, M., Bonazza, M., Capron, E., Castellano, E., Chappellaz, J., Delmonte, B., Falourd, S., Genoni, L., Iacumin, P., Jouzel, J., Kipfstuhl, S., Landais, A., Lemieux-Dudon, B., Maggi, V., Masson-Delmotte, V., Mazzola, C., Minster, B., Montagnat, M., Mulvaney, R.,

Narcisi, B., Oerter, H., Parrenin, F., Petit, J. R., Ritz, C., Scarchilli, C., Schilt, A., Schüpbach, S., Schwander, J., Selmo, E., Severi, M., Stocker, T. F., and Udisti, R.: Expression of the bipolar see-saw in Antarctic climate records during the last deglaciation, Nat. Geosci., 4, 46–49, doi:10.1038/ngeo1026, 2011. 3325, 3331, 3363

Stocker, T. F. and Johnsen, S. J.: A minimum thermodynamic model for the bipolar seesaw, Paleoceanography, 18, 1087, doi:10.1029/2003PA000920, 2003. 3324

Sugden, D. E., McCulloch, R. D., Bory, A. J. M., and Hein, A. S.: Influence of Patagonian glaciers on Antarctic dust deposition during the last glacial period, Nat. Geosci., 2, 281–285, doi:10.1038/ngeo474, 2009. 3341

Tegen, I.: Modeling the mineral dust aerosol cycle in the climate system, Quaternary Sci. Rev., 22, 1821–1834, doi:10.1016/S0277-3791(03)00163-X, 2003. 3340

Toggweiler, J. R.: Variation of atmospheric $CO_2$ by ventilation of the ocean's deepest water, Paleoceanography, 14, 571–588, doi:10.1029/1999pa900033, 1999. 3324

Toggweiler, J. R., Russell, J. L., and Carson, S. R.: Midlatitude westerlies, atmospheric $CO_2$, and climate change during the ice ages, Paleoceanography, 21, PA2005, doi:10.1029/2005pa001154, 2006. 3324

Vallelonga, P., Barbante, C., Cozzi, G., Gabrieli, J., Schüpbach, S., Spolaor, A., and Turetta, C.: Iron fluxes to Talos Dome, Antarctica, over the past 200 kyr, Clim. Past, 9, 597–604, doi:10.5194/cp-9-597-2013, 2013. 3332, 3336

Veres, D., Bazin, L., Landais, A., Toyé Mahamadou Kele, H., Lemieux-Dudon, B., Parrenin, F., Martinerie, P., Blayo, E., Blunier, T., Capron, E., Chappellaz, J., Rasmussen, S. O., Severi, M., Svensson, A., Vinther, B., and Wolff, E. W.: The Antarctic ice core chronology (AICC2012): an optimized multi-parameter and multi-site dating approach for the last 120 thousand years, Clim. Past Discuss., 8, 6011–6049, doi:10.5194/cpd-8-6011-2012, 2012. 3328, 3329, 3362

Wagenbach, D., Ducroz, F., Mulvaney, R., Keck, L., Minikin, A., Legrand, M., Hall, J. S., and Wolff, E. W.: Sea-salt aerosol in coastal Antarctic regions, J. Geophys. Res., 103, 10961–10974, doi:10.1029/97JD01804, 1998. 3326

Wegner, A., Gabrielli, P., Wilhelms-Dick, D., Ruth, U., Kriews, M., De Deckker, P., Barbante, C., Cozzi, G., Delmonte, B., and Fischer, H.: Change in dust variability in the Atlantic sector of Antarctica at the end of the last deglaciation, Clim. Past, 8, 135–147, doi:10.5194/cp-8-135-2012, 2012. 3325

Werner, M., Tegen, I., Harrison, S. P., Kohfeld, K. E., Prentice, I. C., Balkanski, Y., Rodhe, H., and Roelandt, C.: Seasonal and interannual variability of the mineral dust cy-



cle under present and glacial climate conditions, J. Geophys. Res.-Atmos., 107, 4744, doi:10.1029/2002jd002365, 2002. 3340

Wolff, E. W., Rankin, A. M., and Röthlisberger, R.: An ice core indicator of Antarctic sea ice production?, Geophys. Res. Lett., 30, 2158, doi:10.1029/2003GL018454, 2003. 3324, 3326

Wolff, E. W., Fischer, H., Fundel, F., Ruth, U., Twarloh, B., Littot, G. C., Mulvaney, R., Röthlisberger, R., de Angelis, M., Boutron, C. F., Hansson, M., Jonsell, U., Hutterli, M. A., Lambert, F., Kaufmann, P., Stauffer, B., Stocker, T. F., Steffensen, J. P., Bigler, M., Siggaard-Andersen, M. L., Udisti, R., Becagli, S., Castellano, E., Severi, M., Wagenbach, D., Barbante, C., Gabrielli, P., and Gaspari, V.: Southern Ocean sea-ice extent, productivity and iron flux over the past eight glacial cycles, Nature, 440, 491–496, doi:10.1038/nature04614, 2006. 3324, 3330, 3333, 3335, 3336, 3340, 3345

Yang, X., Pyle, J. A., and Cox, R. A.: Sea salt aerosol production and bromine release: Role of snow on sea ice, Geophys. Res. Lett., 35, L16815, doi:10.1029/2008GL034536, 2008. 3326

Yung, Y. L., Lee, T., Wang, C.-H., and Shieh, Y.-T.: Dust: A Diagnostic of the Hydrologic Cycle During the Last Glacial Maximum, Science, 271, 962–963, doi:10.1126/science.271.5251.962, 1996. 3339, 3340

**Table 1.** In the first row the $\Delta t/\tau$ values of EDML vs. EDC for different time periods during the past 150 ka are shown. Below, the fluxes of nss$Ca^{2+}$ and ss$Na^{+}$ (given in $\mu g\,m^{-2}\,a^{-1}$) are indicated for EDC, EDML, and TALDICE, respectively, for the corresponding time intervals.

| Time period (ka BP) | Holocene 3–15 | LGM 15–30 | MIS 3 30–60 | MIS 4–5.4 60–115 | MIS 5.5 115–133 | MIS 6 133–146 |
|---|---|---|---|---|---|---|
| $\Delta t/\tau_{(EDML/EDC)}$ | 1.22 ± 0.61 | 1.19 ± 0.16 | 1.40 ± 0.43 | 1.48 ± 0.39 | 1.54 ± 0.57 | 1.38 ± 0.30 |
| | | | EDC | | | |
| J(nss$Ca^{2+}$) | 22 ± 14 | 414 ± 145 | 141 ± 84 | 118 ± 121 | 30 ± 17 | 384 ± 113 |
| J(ss$Na^{+}$) | 515 ± 134 | 786 ± 142 | 866 ± 112 | 830 ± 161 | 455 ± 187 | 816 ± 205 |
| | | | EDML | | | |
| J(nss$Ca^{2+}$) | 76 ± 49 | 1433 ± 505 | 555 ± 277 | 442 ± 396 | 130 ± 56 | 1559 ± 519 |
| J(ss$Na^{+}$) | 684 ± 245 | 1802 ± 332 | 1656 ± 334 | 1536 ± 310 | 761 ± 417 | 1454 ± 512 |
| | | | TALDICE | | | |
| J(nss$Ca^{2+}$) | 136 ± 86 | 507 ± 138 | 190 ± 93 | 170 ± 138 | 110 ± 68 | 422 ± 132 |
| J(ss$Na^{+}$) | 850 ± 309 | 1336 ± 383 | 1750 ± 323 | 1223 ± 293 | 969 ± 364 | 1279 ± 158 |



**Table 2.** Slopes of the linear regressions calculated for the 10 yr model runs as shown in Fig. 7. The first line indicates the slopes of the dust deposition (Fig. 7d), the second line those of the atmospheric dust load (Fig. 7c). The slopes of the regressions are indicated including the standard deviation, the respective $r^2$ values are indicated in parenthesis.

| | EDC vs. Vostok | EDC vs. EDML | EDC vs. TALDICE |
|---|---|---|---|
| Deposition | 0.93 ± 0.06 (0.94) | 1.64 ± 0.19 (0.80) | 0.75 ± 0.10 (0.77) |
| Load | 1.04 ± 0.01 (0.999) | 1.57 ± 0.06 (0.98) | 0.99 ± 0.01 (0.997) |

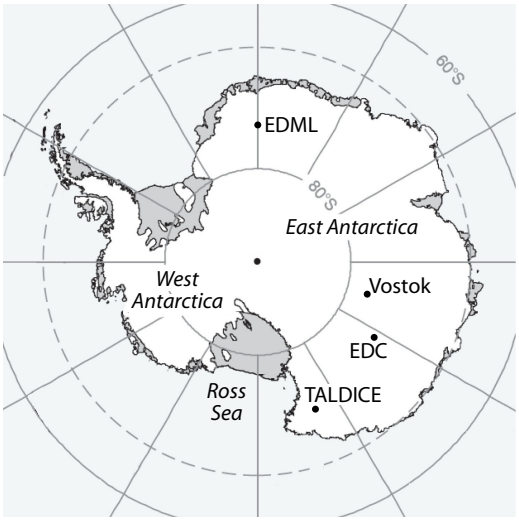


**Fig. 1.** The four Antarctic drilling sites discussed in this work are indicated. One is located in the Atlantic sector (EDML) and, thus, closer to the SSA continental dust source than EDC and Vostok, both being located in the Indian Ocean sector. The fourth drilling site, TALDICE, is at a more coastal site close to the Ross Sea and therefore also influenced by local source regions and wind patterns especially during warm periods (see text for more information).



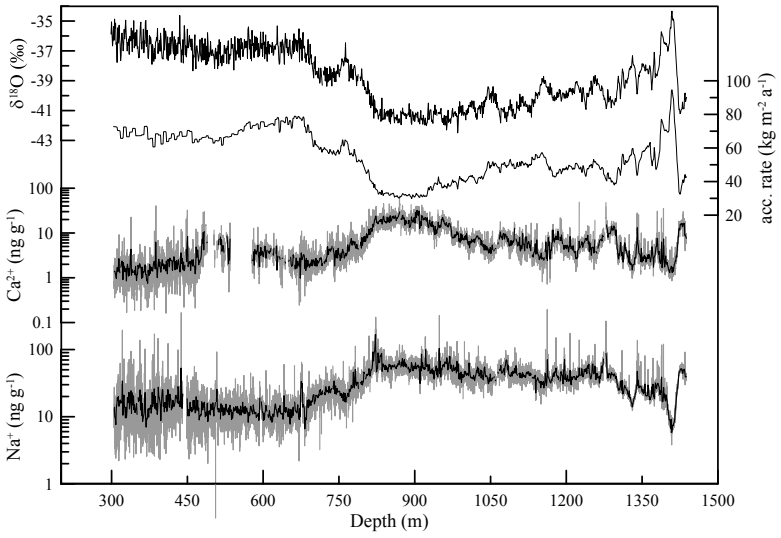


**Fig. 2.** The $\delta^{18}O_{ice}$ profile of TALDICE (Stenni et al., 2011) is shown in the top panel. In the second panel the accumulation rate is shown as modeled in the recent AICC2012 age scale for Talos Dome (Bazin et al., 2012; Veres et al., 2012). The third and fourth panels show TALDICE $Ca^{2+}$ and $Na^{+}$ concentrations, respectively (new data); note the logarithmic scale for both aerosol records. Black lines indicate 1 m mean values, grey lines indicate 10 cm mean values, both calculated from the high-resolution CFA data. All data are plotted versus depth along the Talos Dome ice core.

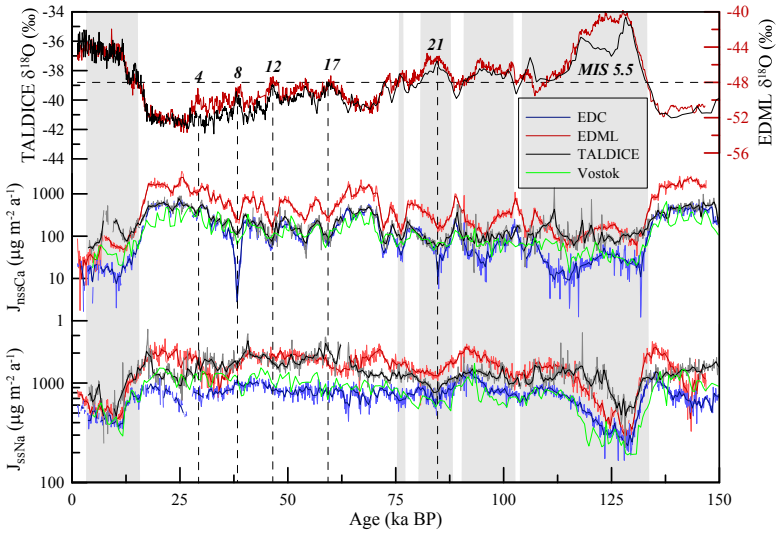


**Fig. 3.** Top panel: the $\delta^{18}O_{ice}$ profile of TALDICE (Stenni et al., 2011) and EDML (EPICA, 2006) are shown to illustrate the temperature evolution at the two drill sites. The dashed horizontal line indicates the TALDICE temperature threshold ($\delta^{18}O_{ice}$ = −38.9 ‰) to discriminate warm and cold periods, respectively (see text for explanation), accordingly the gray shadowed areas indicate warm periods ($\delta^{18}O_{ice}$ above threshold). Major AIM events (EPICA, 2006) are indicated by numbers above the curve, the dashed vertical lines indicate the maxima of the corresponding AIM events. Middle panel: the nss$Ca^{2+}$ flux of TALDICE (new data) is plotted in black along the one of EDC (blue) (Bigler et al., 2006), EDML (red) (Kaufmann et al., 2010), and Vostok (green) (De Angelis et al., 1997), respectively. Bottom panel: the ss$Na^{+}$ flux of TALDICE (new data) is plotted in black along the one of EDC (blue) (Bigler et al., 2006), EDML (red) (Kaufmann et al., 2010), and Vostok (green) (De Angelis et al., 1997), respectively. Light colors indicate 100 yr median values, dark colors 500 yr median values.



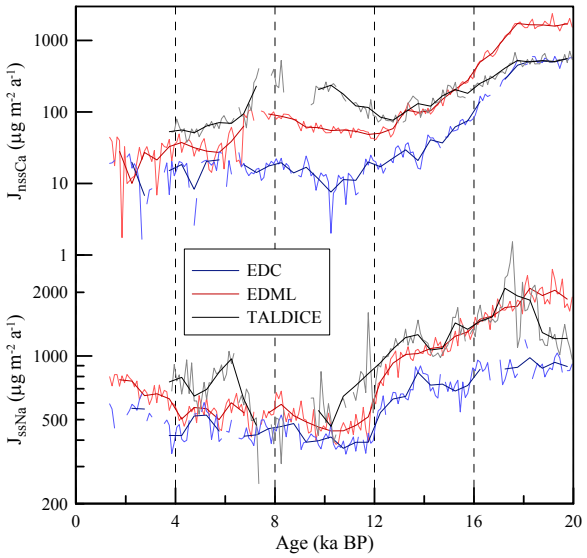


**Fig. 4.** Nss$Ca^{2+}$ and ss$Na^{+}$ fluxes are shown during the Holocene and T1. It is evident that in TALDICE they show an anticorrelated behaviour during the deglaciation and early Holocene, i.e. 13–8 ka BP. This supports the scenario by Albani et al. (2012a) who suggest a change from air masses originating from local terrestrial dust sources (13–8 ka BP) to such passing over the Ross Sea after ≈ 8 ka. Such change in local atmospheric circulation patterns could explain the transition from relatively high nss$Ca^{2+}$ and low ss$Na^{+}$ from 12–8 ka BP towards low nss$Ca^{2+}$ and high ss$Na^{+}$ after 8 ka BP in TALDICE.

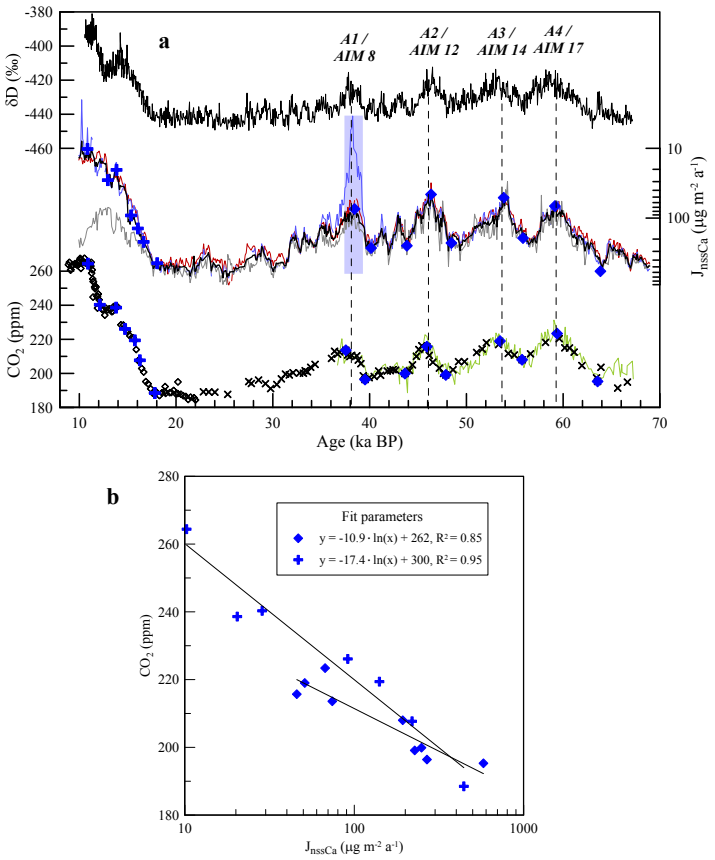




**Fig. 5. (a)** The same data as in Fig. 1 of Röthlisberger et al. (2004) are shown in the top panel, EDC $\delta$D, and in the bottom panel, $CO_2$ concentrations of EDC (diamonds) and of Taylor Dome (crosses). More recent EDML and TALDICE $CO_2$ concentrations (Bereiter et al., 2012) are shown for comparison (green line). The middle panel shows the mean $nssCa^{2+}$ flux calculated from the 100 yr medians of EDC, EDML, and TALDICE, respectively (black line); discarded EDC values during AIM 8 are marked by the blue shaded area. Blue diamonds and crosses in the bottom panel indicate the same tie points used for the linear regression calculation as done by Röthlisberger et al. (2004). In addition, the 100 yr means of EDC (blue line), normalised EDML (red line), and TALDICE (gray line) are shown in the middle panel. **(b)** Linear regressions of the blue diamonds and crosses from **(a)**, according to Röthlisberger et al. (2004). Due to the discarded EDC values during AIM 8, which biased the regression calculated by Röthlisberger et al. (2004) based on EDC values significantly, we obtain a regression line of the diamonds (representing $CO_2$ and $nssCa^{2+}$ during A4–A1) much closer to the one during the transition from the LGM into the Holocene, indicated by the crosses. This shifts the estimate of the impact of dust induced iron fertilisation in the SO on $CO_2$ changes during the transition from up to 20 ppm as calculated by Röthlisberger et al. (2004) to up to 40 ppm based on our $nssCa^{2+}$ composite record from EDC, EDML, and TALDICE, respectively.

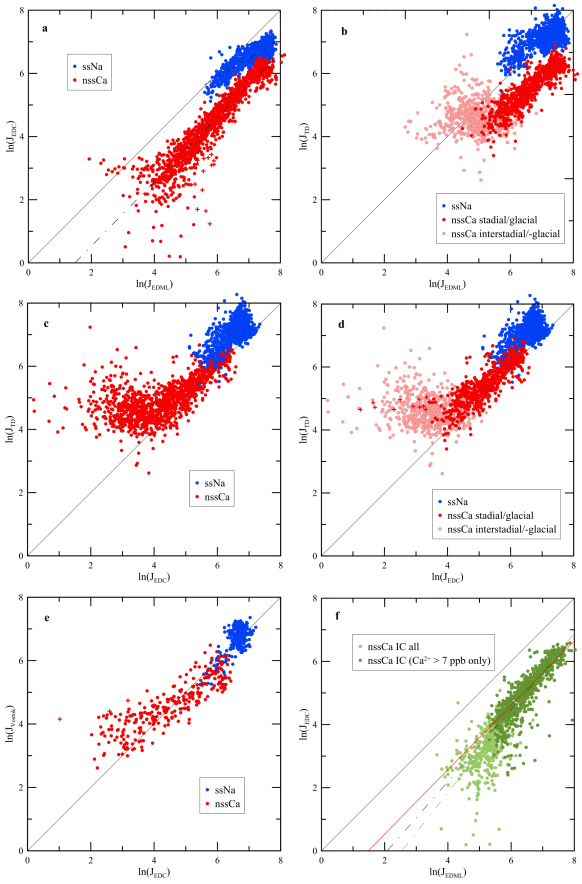




**Fig. 6.** Double-logarithmic scatter plots of the nssCa$^{2+}$ (red) and ssNa$^{+}$ (blue) fluxes in 100 yr resolution (500 yr resolution for Vostok only). **(a)** EDC vs. EDML. The linear regression (dash dotted lines) shows a slope of 1 for nssCa$^{2+}$ and of 0.6 for ssNa$^{+}$. Outliers of the AIM 8 event are indicated as red crosses (see text for explanation). **(b)** TALDICE vs. EDML. Cold (dark red dots) and warm periods (light red dots) are discriminated in the nssCa$^{2+}$ scatter. **(c)** TALDICE vs. EDC. The strong correlation of **(a)** is no longer persistent with these two ice cores when considering all climate periods of the past 150 ka. **(d)** TALDICE vs. EDC. The same data as in **(c)**, however, cold (dark red dots) and warm periods (light red dots) are now discriminated. It becomes evident that during cold periods the linear correlation is still persistent, while for warm periods the two records are completely uncorrelated. EDC outliers during AIM 8 are indicated with red crosses. **(e)** Vostok vs. EDC. Vostok data were analysed using IC, thus, low nssCa$^{2+}$ fluxes are biased towards higher values in the Vostok record – same effect as seen in **(f)**. Data are shown in 500 yr resolution only. **(f)** EDML IC data versus EDC CFA data as shown in Fischer et al. (2007a) (here on the AICC2012 age scale with its respective accumulation rate). All data are shown in light green, in dark green only the data with original Ca$^{2+}$ concentrations higher than 7 ppb. Linear regressions (dash-dotted lines) through all the IC data (light green, slope of the regression is 1.26) and those above the 7 ppb threshold only (dark green, slope = 1.13) show that the IC data set is indeed approaching the slope of the CFA data set as in **(a)** (red line, slope = 1.02), when low concentration IC values are discarded.

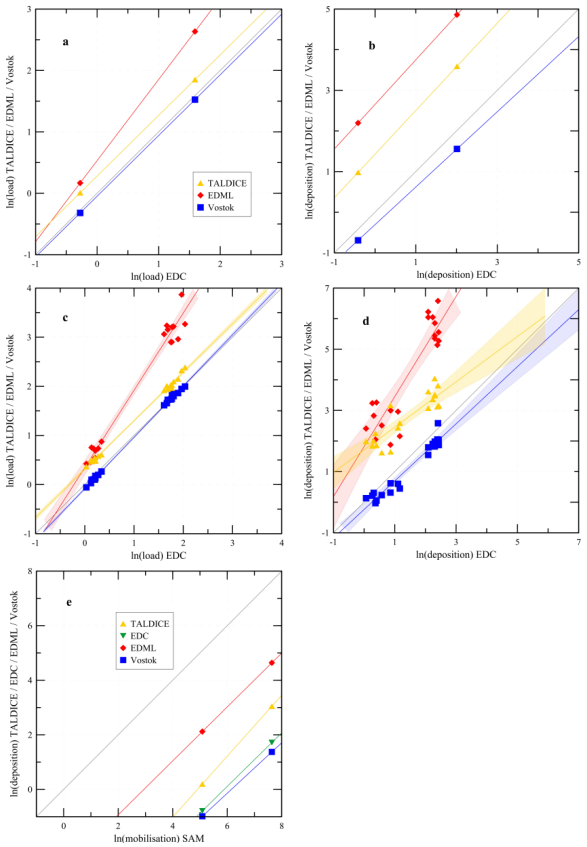




**Fig. 7. (a)** Dust column loadings (load) of 1 yr tuned model runs (Albani et al., 2012b). Double-logarithmic plots of EDML (red diamonds), Vostok (blue squares), and TALDICE (yellow triangles) versus EDC. **(b)** Double-logarithmic plots of modelled dust deposition for all drill sites. The results are from the same model run as in **(a)**. **(c)** Results of two 10 yr simulations showing inter-annual variability (10 points for each climate period) of the dust column loadings (load). Double-logarithmic scatter plots of EDML (red diamonds), Vostok (blue squares), and TALDICE (yellow triangles) versus EDC, with the linear regressions including significance intervals (95 %) indicated in respective colours. See Table 2 for slopes, standard deviations, and $r^2$ values of the regressions shown in this figure. **(d)** Double-logarithmic plots of two 10 yr simulations for all drill sites showing inter-annual variability of the dust deposition. The results are from the same model run as in **(c)**. Linear regressions including significance intervals (95 %) are indicated in respective colours. **(e)** This double logarithmic scatter plot of the source mobilisation vs. deposition shows the relation of dust originated and deposited to the four ice core sites from a unique source (South America, SAM) based on the 1 yr tuned case of Albani et al. (2012b). Green triangles represent EDC.